Massive surface membrane expansion without involvement of classical exocytic mechanisms.

Michael Fine[1], Christopher Bricogne[2], and Donald Hilgemann[1]

Author Affiliation:

[1] University of Texas Southwestern Medical Center, Department of Physiology, Dallas, Texas, USA

[2] UCL Cancer Institute, University College London, Gower St, London, UK.

Corresponding author: Donald.Hilgemann@utsouthwestern.edu;

Abstract

TMEM16F activation induces a transient cation conductance, extracellular exposure of anionic phospholipids, and the opening of deeply invaginating membrane compartments that contain VAMP4. Membrane expansion can occur with one micromolar free Ca_i^{2+} and requires monovalent cations (Na≈K≈Cs>n-methyl-d-glucamine>>TEA). Membrane expansion can be reversed by substituting extracellular ions for sugars. Closure is also favored by inward cation gradients. Depolarization tehn fully closes the compartments while hyperpolarization reopens them. Cationic peptides that bind anionic phospholipids open the compartments from the cytoplasmic side without Ca^{2+} and promote Ca^{2+}-dependent openings from the extracellular side. In summary, TMEM16F-mediated membrane expansion reflects the relaxation of membrane binding proteins that constrict the necks of invaginating membranes by binding anionic phospholipids.

Introduction

Eukaryotic cells use exocytosis and endocytosis to increase and decrease their surface membrane areas, thereby transferring chemicals to and from the extracellular space and modifying the protein content of the surface membrane (Sudhof and Rothman, 2009) . Besides these functions, surface membrane expansion may become essential to allow cell growth (Tojima et al., 2014), to allow cell swelling (Groulx et al., 2006), and to repair membrane wounds in the surface membrane (Cooper and McNeil, 2015; Corrotte et al., 2015; Moe et al., 2015) .

Multiple cell types are able to increase their membrane area by up to two-fold within a few seconds in response to large elevations of cytoplasmic Ca (Wang and Hilgemann, 2008; Yaradanakul et al., 2008; al., XXXX). We have also described previously that synaptotagmins are unlikely to be the Ca sensors in these large-scale cell responses (Wang and Hilgemann, 2008). Rather, as shown in an accompanying article, that these large-scale cell responses are likely initiated by Ca activation of the membrane protein, TMEM16F (al., XXXX). When activated by Ca, TMEM16F appears to function simultaneously as a nonselective cation channel and phospholipid scramblase (Suzuki et al., 2013; Fujii et al., 2015; Scudieri et al., 2015). Here, we analyze how these functions are involved in membrane expansion. The experiments to be described contradict the idea that membrane expansion reflects *bona fide* membrane fusion events. Rather, it appears that the membrane structures which expand the surface membrane are in fact contiguous with the surface membrane prior to Ca activation of TMEM16F. However, they are electrically isolated from the surface membrane by constrictions that effectively close the submembrane compartments involved and hinder conduction of ions into their lumens. The invaginating structures are in general too large to reflect caveoli (Shaul and Anderson, 1998) , although an involvement of caveoli cannot be discounted at this time. Membrane compartments dubbed enlargeosomes (Cocucci et al., 2007; Cocucci et al., 2008; Racchetti et al., 2012) appear more consistent with our morphological analysis, although we cannot support the idea that membrane expansion involves exocytosis Pcocucci,2008}. Rather, out data indicate that loss of anionic phospholipids from the cytoplasmic membrane leaflet by scramblase activity, or by neutralization with cationic peptides, causes a release of the constrictions that close these compartments and thereby their reversible opening to the extracellular space. This hitherto unappreciated mechanism of surface membrane expansion is likely to be of widespread biological import and may also be operative in cell types that do not express TMEM16F.

Results.

Overview of working hypotheses. Fig. 1 illustrates the working hypotheses to be advanced in this article. As will be shown in Figs. 2 to 4, the membrane compartments that expand the surface membrane during TMEM16F activity usually extend deeply into cells and appear to be constricted in regions where they converge with the outer surface membrane (see Fig. 1A). As will be described in Figs. 6 to 11, the opening of these compartments is reversible and therefore cannot reflect bona fide membrane fusion events. Rather, we propose that membrane proteins that bind anionic phospholipids constrict the necks of these compartments to such an extent that they become isolated electrically from the extracellular space. Activation of TMEM16F effectively opens the compartments by allowing anionic phospholipids to escape to the extracellular monolayer, thereby promoting the relaxation of constrictions that rely on cation membrane protein domains that bind anionic phospholipids. As illustrated in Fig. 1B, we propose that TMEM16F exists in primarily three activity states. In the absence of cytoplasmic Ca, channels are closed and inactive. Upon activation by cytoplasmic Ca, the open channels conduct monovalent cations and anionic phosphoplipids, and likely also conduct other phospholipids. Conduction of anionic phospholipids requires the presence of monovalent cation in the channel pore. Specifically, the entrance of anionic phospholipids into the channels requires that a monovalent cation is bound near the entrance to the channel, at the orifice into which the anionic phospholipid enters. The monovalent cation is then assumed to accompany the anionic phospholipid through the channel in an electroneutral fashion. Accordingly, occupancy of channels by nonvalent cations, but not the permeation of monovalent cations per se, is required for scrambling of negatively charge lipids. Finally, we propose that TMEM16F channels, like many anion channels, are activated secondarialy by anionic phospholids binding to regulatory sites on the cytoplasmic side, independent of phospholipid scrabling. Accordingly, channel activity and scramblase activity inactivate as anionic phospholipids are lost from cytoplasmic leaflet to the extracellular leaflet.

Optical characterization of TMEM16F-mediated surface membrane expansion. In a previous study we attempted to identify the membrane compartments that putatively fuse during high Ca responses in BHK cells using electronmicroscopy. In short, there was a large discrepancy between the numbers of secretory vesicles that could be identified within close proximity to the surface membrane and the magnitude of membrane expansion that could occur in less than 5 s. Furthermore, membrane expansion did not bring ion transporters such as Na/K

pumps and constitutively over-expressed Na/Ca exchangers into the surface membrane. As described in the accompanying article, endoplasmic reticulum does not become involved membrane expansion, nor are acidified lysosomes involved. These results seen inconsistent with involvement of conventional secretory compartments, and the discrepancies led us to consider the involvement of deeper membrane compartments. In this connection, we observed that FM dyes often reversibly label membrane compartments that extend deeply into BHK cells after Ca^{2+} elevations. Given that FM4-64 fluorescence increases over-proportionally to C_m (i.e. membrane expansion), we tested whether other dyes might allow more reliable visualization of the compartments that expand the surface membrane. As described in Fig. 2, we found that the impermeant dye, Trypan blue (TB) , which binds to surface sugars and proteins without inserting into the membrane (Harrisson et al., 1981), indeed routinely stains deep, invaginating membrane compartments after large Ca^{2+} elevations generated by reverse Na/Ca exchange (Yaradanakul et al., 2008).

As described in Fig. 2A, we tested TB in our standard protocols to cause membrane expansion and MEND, using both WT and TMEM16F-null Jurkat cells. Here and for all subsequent experiments, the detailed composition of solutions is available in Materials and Methods. Using Cytoplasmic Solution #1 and Extracellular Solution #1 (i.e. normal cation gradients), TB fluorescence shifts correlated linearly with C_m changes in these protocols, generating a Pearson correlation coefficient of 0.9 and slope of 0.96 ±0.03. In further experiments, Jurkat cells were patched and labelled with TB to determine the initial depth of reversible membrane staining (Figs. 2B-2E). Cells were then washed, stimulated with Ca^{2+}-ionophore, and relabeled with TB to determine any change in membrane depth (Fig. 2B and 2C). As shown in Figs. 2D and 2E, Wildtype Jurkat and HEK293 cells exhibit increased TB labelling that extends on average 2.6 and 2.1 µm into the cell, respectively. In the absence of TMEM16F, neither cell type exhibited a change in labelling depth after the Ca application. Fig. 2F shows results for an NCX1-expressing BHK cell in which membrane expansion was initiated by reverse exchange activity. In this case, membrane labelling with Trypan blue clearly extends many microns into membrane compartments of substantial (>3 µm) dimensions.

Novel properties of TMEM16F-induced membrane expansion. Fig. 3 illustrates the development of membrane expansion over several minutes when cells are patch clamped with highly Ca-buffered cytoplasmic solutions (Cytoplasmic Solution #2. 5 mM EGTA with 4.6 mM Ca; ~4 µM free Ca^{2+}; Extracellular Solution #2). Simultaneously, we applied a cationic peptide, hexalysine-rhodamine (K7r), to visualize the exposure of anionic phospholipids in the outer

monolayer and the morphology of membrane compartments that expand the cell surface. From previous work (Yaradanakul et al., 2008), it is known that K7r requires exposure of anionic phospholipids in the outer monolayer to bind to the cell surface. As evident in these records, anionic lipids become exposed as membrane expansion proceeds to >50% of membrane area, and the time courses of the two processes are similar. Line scans of the K7r fluorescence illustrate further that K7r binding extends deeply into the cell, similar to results for TB.

As concerns the identity of membrane that expands the cell surface, the results of Fig. 2 appear for the most part consistent with reports that novel organelles, dubbed enlargeosomes, expand the cell surface during high Ca responses in some cell types, such as PC12 cells (Cocucci et al., 2007; Cocucci et al., 2008). In this connection, the SNARE protein VAMP4 was reported to be a relatively enriched marker of the organelles that expand the cell surface (Cocucci et al., 2008). Therefore, we expressed VAMP2,4 and 7constructs with a pHluorin fusion in BHK cells to test whether these proteins indeed enter the surface membrane during membrane expansion. As shown in Fig. 4 (Cytoplasmic Solution #3, Extracellular Solution #2), we applied Trypan blue to image the surface membrane and to quench extracellular fluorescence of the VAMP proteins in the surface membrane, before and after membrane expansion was initiated by Ca influx via constitutively expressed Na/Ca exchangers. The membrane expansion induced by Ca influx amounted to ~60% in all experiments experiment. Before membrane expansion, application of 1 μM TB resulted in strong quenching of the VAMP2 and VAMP7 fluorescence, but only weak quenching of VAMP4 fluorescence. From the three VAMPs, the VAMP4 signal increased most strongly (~60%) and the subsequent application of TB then quenched the Vamp4 signal by about 25%. We conclude on this basis that overexpressed VAMP4 proteins indeed localize to the membrane compartment that expands the surface membrane.

Membrane expansion can be activated by 1 μM free Ca^{2+}. Figures 5 and 6 describe further properties of membrane expansion during TMEM16F activation. Previously, we described that the $K_{1/2}$ for activation of membrane expansion by Ca is about 20 μM in BHK cells (Yaradanakul et al., 2008). Since however the Ca dependence does not show significant cooperativity, membrane expansion proceeds slowly but effectively at relatively low cytoplasmic free Ca concentrations. As illustrated in Fig. 5A, membrane expansion results in a full 40% increase of membrane area over 10 min when the cytoplasmic solutions are buffered heavily to 1 μM free Ca (30 mM EGTA, 20 mM Ca, pH 7.0, with no Mg and 2 mM of the nonhydrolyzable ATP analogue, AMPPCP; Cytoplasmic Solution #4, Extracellular Solution #4). No membrane expansion occured in the absence of Ca and expansion was blocked by 80% when 1 mM

spermine was included in the cytoplasmic solution to block TMEM16F activity (al., XXXX). Using Jurkat cells in Fig. 4B, we found that a somewhat higher free Ca was required (3 μM; 30 mM EGTA with 26 mM Ca) to elicit reliable membrane expansion. We stress in this connection that Jurkat cells lost about 18% of their membrane area over 10 min when perfused with Ca-free solutions solutions. In TMEM16F-null Jurkat cells, the same cytoplasmic solution with 3 μM free Ca, which evoked a 25% increase of membrane area in WT cells, evoked nearly a 40% loss of membrane area over 10 min, as expected from our accompanying study (al., XXXX). These results underscore that membrane expansion by TMEM16F does not require excessively high free Ca, as expected to occur during membrane wounding.

Membrane expansion by TMEM16F activation is reversible. Next, we address the key mechanistic question of this study, whether membrane expansion indeed reflects fusion of submembrane vesicles with the cell surface, as occurs during neurotransmitter release, or might rather occur via an alternative mechanism. The alternative, already outlined in Fig. 1, is that membrane expansion reflects the opening of membrane compartments that are in fact contiguous with the cell surface but are closed by constrictions occurring close to the outer cell surface. A first line of evidence for this hypothesis is presented in Fig. 6 (Cytoplasmic Solution #3, Extracellular Solution #2). As background to these experiments, sugars are known to decrease the lateral mobility of phospholipids in membrane bilayers (van den Bogaart et al., 2007)and we reasoned there fore that substitution of ions for sugars might promote membrane-membrane interactions that close the submembrane compartements. As illustrated in Fig. 6A, membrane expansion induced by Ca influx via Na/Ca exchangers in BHK cells can be rapidly and quantitatively reversed by removing most of the monovalent ions and substituting them for sugars. Upon applying trehalose (Extracellular Solution #5), C_m decreased within 4 s by 75% of the maximal membrane expansion that occurred during Ca influx (n=9). Fig. 6B illustrates the results of all 9 experiments. In those cases in which membrane expansion amounted to less than ~50% of membrane area, the response to trehalose reversed upon reapplying ions. In those cases in which membrane expansion responses were greater than ~50%, the reversal of expansion by trehalose remained stable upon removing trehalose and reapplying ions. The fact that membrane expansion can be rapidly reversed in these experiments provides a strong first argument that fusion of membranes, which is in general expected to be an irreversible process, may not be the mechanism of membrane expansion in these experiments.

Relationships between TMEM16F conductance and membrane expansion.

Figure 7 describes in Jurkat cells the detailed relationships between membrane expansion, as monitored via capacitance (C_m) changes, membrane current (I_m) and membrane conductance (G_m) when Ca was elevated by applying ionomycin (5 μM) for up to 1 min. As shown in Fig. 7A (Cytoplasmic Solution #1, Extracellular Solution #1), the time course with which C_m rises follows closely the time course of membrane current (I_m) and conductance (G_m). Specifically, the integral of the G_m signal matches very closely the time course of the C_m signal, as illustrated in the upper records (>20 observations). Therefore, we next tested whether TMEM16F-conduction of ions might be required for membrane expansion and/or might modify membrane expansion. To do so, we replaced cytoplasmic and extracellular ions with aspartate (Asp), *N*-methyl-d-glucamine (NMG), or isotonic sucrose (Fig. 7B; Cytoplasmic Solution #3; Extracellular Solution #2). The presence of either cytoplasmic Na (40 mM in Fig. 7B) or K supported large-scale membrane expansion in the absence of Cl, while expansion responses were smaller without Na or K on the cytoplasmic side. Responses were reduced by ~50% from control responses when Na^+ and K^+ were replaced with equimolar NMG-Asp on both membrane sides, and they were reduced to ~20% when TEA-Asp was employed on both membrane sides. Replacement of 90% of ions with isotonic sucrose fully blocked exocytosis.

Since the changes of membrane expansion roughly correspond to the relative permeabilities of Na, K, NMG, and TEA in TMEM16F channels (Yang et al., 2012), we tested next whether membrane expansion might be coupled to the rate of ion permeation. In experiments illustrated in Fig. 7C, we employed 30 mM Na on the cytoplasmic side in the presence of NMG-Asp on both sides. With these solutions, membrane expansion is limited in rate and extent by the cytoplasmic Na concentration. In contrast to the conditions of Fig. 7A with physiological ion compositions, large (>2 nA) outward Na currents are generated in this condition. Holding membrane potential at +50 mV, ionomycin induced a large transient conductance, as in Fig. 7A, which per usual developed and decayed with the same time course as membrane expansion. When membrane potential was held at -50 mV, however, the conductance was strongly suppressed, as were membrane currents, but membrane expansion proceeded to the same extent (ΔC_m), occurred with a similar time course, and achieved the same maximal rate ($\Delta C_m/dt$) as at +50 mV. Composite results (n=6) shown in Fig. 7D unambiguoulsy dissociate ion conduction *per se* from membrane expansion. The results also negate a possibility that Ca^{2+} influx via TMEM16F could be initiating the membrane expansion because, in that case, hyperpolarization would be expected to enhance Ca^{2+} influx and thereby enhance the

progression of membrane expansion. Rather, another function of TMEM16F triggered by Ca^{2+} must underlie the activation of membrane expansion.

Anionic phospholipid scrambling and membrane expansion require monovalent cations. As just illustrated, ion permeation through TMEM16F has per se no influence on membrane expansion, although the time course of membrane expansion reflects the time course of TMEM15F activation and inactivation. As introduced in Fig. 1B, our working hypothesis is that monovalent cations must occupy the TMEM16f channel pore to allow the entrance of anionic phospholipids into the channel. Accordingly, the presence of extracellular or intracellular cations can potentially facilitate the movement of anionic phospholipids through the channel in either direction. Furthermore, it is expected that, when large monovalent cation gradients are imposed, unnaturally, the cation gradient can provide an energy that promotes movement of anionic phospholipids in the direction of the gradient.

Simple predictions of this working hypothesis are provided in Fig. 8 as simulations that are described in Material and Methods. Fig. 8A illustrates the basic response of the model to a step increase of free cytoplasmic Ca from 0 to 20 μM. Using an outward monovalent cation gradient solutions with 40 mM extracellular Na and 140 mM cytoplasmic Na, TMEM16F channels generate an outward current that inactivates ~90% as PS is lost from the cytoplasmic leaflet to the extracellular leaflet. Nearly all of the subsurface membrane compartements are predicted to opend. Fig. 8B depicts the activation of scrambling and membrane expansion by extracellular cations when the cytoplasmic solution contains no cations that facilitate PS movement into the channel (i.e. 140 mM TEA_i). Each curve in the figure depicts the fractions of membrane compartments predicted to be open as a result of anionic phospholipids being lost from the cytoplasmic to the extracellular leaflet. Specifically, it is assumed that 4 phosphatidylserine (PS) molecules must be bound by protein 'grippers' that hold the compartments shut, and it is assumed that the grippers are half-saturated with PS at approximately the resting concentration of PS in the inner monolayer. The cytoplasm was assumed to contain only 20 mM Na, with120 mM TEA, while the extracellular solution initially contains 140 mM TEA and no other monovalent cation. Thus, only cytoplasmic Na can bind to and interact with the TMEM16F channels. Cytoplasmic free Ca is assumed to be 3 μM subsequent to the 20 s point in the simulation. For the four simulations, extracellular TEA was assumed to be substituted for extracellular Cs at the four different time points as indicated. Early substitution of TEA for Cs promotes compartment opening to proceed to a steady state value of about 70% of all available compartments. When extracellular Cs is applied at later time points, the PS gradient can be partially re-established as

the Cs gradient forces PS backward from the extracellular to the cytoplasmic leaflet. Maximally, a reversal of about 30% of the total number of available compartments can be achieved with 140 mM extracellular Cs.

Figure 9 illustrates these predictions from experiments in which either extracellular Na (Figs. 9A and B) or extracellular Cs (Figs. 9C and D) were used to slow and/or reverse membrane expansion (Cytoplasmic Solution #5, Extracellular Solution #4). Cytoplasmic free Ca was heavily buffered with 30 mM EGTA to 3 μM (30 mM EGTA/25 mM Ca). Fig. 9A illustrates the case that membrane expansion was initiated with 20 mM cytoplasmic Na and 140 mM extracellular TEA with 3 μM free Ca. Substitution of TEA for 140 mM Na on the outside effectively stops membrane expansion, as in the 2nd simulation in Fig. 8. Fig. 9B illustrates the simulation in which membrane expansion is allowed to proceed to nearly its maximal extent with 3 μM free Ca. In this case, membrane expansion reverses by about 25% upon substituting extracellular TEA for Cs, and expansion can be reactivated by the reverse concentration change. Using Cs to substitute for TEA in Fig. 9C, Cs initially stops membrane expansion at an intermediate value. After expansion is allowed to proceed further in the presence of TEA, Cs causes an approximately 25% reversal of membrane expansion, similar to results for extracellular Na in Fig. 9B. Fig. 9D illustrates in more detail the speed with which membrane area changes can be reversed by applying and removing Cs in these experiments. Just a few seconds are adequate to establish the maximal rates of membrane area change.

Membrane expansion can be reversed by depolarization. A second means to reverse membrane expansion arises from considering that monovalent ion gradients in the TMEM16F channel will be dependent on voltage. Pronounced effects of membrane potential will arise when the extracellular solution contains high concentrations of monovalent cations and the cytoplasm contains no monovalent cations. Simulations are shown in Fig. 10 for the case that the cytoplasmic solution contains 140 mM TEA and the extracellular solution contains 140 mM Cs. Progressive depolarization of the membrane then clears Cs that occupies the cytoplasmic end of the permeation pathway, resulting in inhibition of scrambling of anionic phospholipids and increased probability that anionic phospholipids can traverse the channel in the inward direction. Hyperpolarization, thererfore, can now promote scrambling by promoting occupation of sites near the cytoplasmic mouth of the channel where anioinic lipids enter the channels. Fig.10A illustrates results for substituting extracellular TEA for Cs at three different membrane potentials.

Results are consistent with hyperpolarization favoring scrambling and thereby opening of the deep membrane compartments. Fig. 10B illustrates the major predictions that (1) depolarization by just 50 mV can largely reverse membrane expansion under these conditions, and (2) that membrane hyperpolarization can again promote membrane expansion

Figure 11 illustrates equivalent experiments results employing TEA as sole monovalent cation in cytoplasmic solutions and employing 5 mM EGTA with 0.47 mM Ca to generate a cytoplasmic free Ca of ~5 μM. In Fig. 11A, the exposure of anionic phospholipids in the outer monolayer was monitored as binding of the K7r peptide, and membrane expansion was monitored via Cm recording. Initially, an extracellular solution containing 140 mM TEA was employed. The K7r signal was small and stable at the onset of the experiments, and the C_m signal was similarly stable for 3 min. Thereafter, 140 mM Cs was substituted for TEA in the extracellular solution. After a delay of 1 min, C_m began to rise and continued to increase nearly linearly for several min to a plateau ~80% greater than the initial C_m. During this same time, the K7r signal increased by ~2-fold. Per usual, deeply invaginating membrane compartments became visible, and the K7r staining could be fully washed off (not shown). These results confirm our working hypothesis that scrambling of anionic phospholipids requires monovalent cations within the channel pore, specifically at sites near the cytoplasmic entrance of the pore.

Figure 11B illustrates the second major prediction, namely that depolarization by 50 mV can largely reverse membrane expansion under these conditions. Using 140 mM Cs on the extracellular side and 140 mM TEA on the cytoplasmic side with free Ca clamped to 5 μM, as in Fig. 11A, membrane potential was stepped to + 50 mV for 2 min, and then to -50 mV for several minutes in 5 experiments. To eliminate any role for ATPase activities, the cytoplasmic solutions contained no Mg and 2 mM of the nonhydrolyzable ATP analogue, AMPPCP. After opening cells at 0 mV, the surface membrane expands from 68 to 88 pF over 4 min. During subsequent depolarization by 50 mV, membrane expansion continues for a few seconds and then reverses almost to baseline within 1 min. Upon subsequent hyperpolarization to -50 mV the membrane again expands without delay, and expansion proceeds beyond the previous expansion at 0 mV. The fact the membrane expansion does not immediately begin to reverse upon depolarization is readily explained by the expectation that Cs may accumulate in the cytoplasm by a few millimolar in the prolonged presence of 140 mM extracellular Cs. The residual cytoplasmic Cs will require a few seconds to be cleared from the cytoplasm during depolarization. The reversible nature of membrane expansion, documented in both Figs. 9 and 11, strongly

contradict the idea that membrane fusion events underlie membrane expansion in these experiments.

Cationic peptides activate membrane expansion from the cytoplasmic side. Next, we examined in more detail how phospholipid scrambling, specifically the loss of cytoplasmic anionic phospholipids, could cause membrane compartments attached to the cell surface to open. Our working model, described in Fig. 1, is that proteins which bind anionic phospholipids can function as a vice at the necks of vesicles and hold the compartments closed to an extent that isolates them electrically from cytoplasm. A major prediction of this model is that chelation of anionic phospholipids on the cytoplasmic side by cationic peptides should release the putative membrane protein grippers. As shown in Fig. 12, this is indeed the case. In these, experiments, the cytoplasmic solution contained 10 mM EGTA with no added Ca, no added Mg, no ATP, and no GTP (Cytoplasmic Solution #5 with 10 EGTA and no Ca, Extracellular Solution #4). As shown in Fig. 12A, C_m increased over 3 min by 30% in BHK cells when the cells were opened in the presence of 3 mg/ml protamine. As shown in Fig. 12B, C_m increased over 3 min by 37% when BHK cells were opened in the presence of 0.2 mM K7r in the cytoplasmic solution. As shown in Fig. 12C, C_m increased by 40% over 2 min when Jurkat cells were opened in the presence of 3 mg/ml protamine.

PS gradients can drive and reverse membrane expansion. A final major prediction of the working hypotheses outlined in Fig. 1 is that removal of PS from extracellular side should shift PS from the cytoplasmic side to the extracellular side and thereby favour membrane expansion. Conversely, enrichment of the cytoplasmic leafet with PS should reverse membrane expansion. As shown in Fig. 13 A, we enriched cells with PS by applying 1:2 PS:albumin complexes (Bartholow and Geyer, 1982) prepared by sonication of PS with albumin in distilled water. As illustrated, using cytoplasmic solutions with 3 μM free cytoplasmic Ca 20 mM EGTA/18 mM Ca), membrane expansion amounted to 35% on average in these experiments. Application of 120 μM albumin-PS complexes resulted in complete reversal of membrane expansion after a delay about 3.5 min. In fact, C_m values decreased significantly below baseline, as expected if PS activated significant endocytic responses in addition to reversing membrane expansion.

Figure 13B illustrates one last prediction of our working hypotheses. From multiple observations described in this article, we predict that anionic phospholipids come nearly to an equilibrium between outer and inner monolayers when TMEM16F channels are open for a few 10 s of seconds. Accordingly, the presence of substances (e.g. peptides) that bind anionic

phospholipids on the extracellular side should promote the loss of anionic phospholipids from the cytoplasmic leaflet and thereby promote membrane expansion. As shown in Fig. 13B, this is indeed the case in BHK cells in which we use Na/Ca exchangers to mediate Ca influx and thereby activate TMEM16F. In this set of experiments, we compared membrane expansion responses in the presence of and the absence of 3 mg/mL protamine in the extracellular solution (Cytoplasmic Solution #3, Extracellular Solution #2). Membrane expansion responses during application of 1 mM Ca for 2 min were approximately doubled ($p=0.021$) in the presence of extracellular protamine versus the absence of protamine, while peak Na/Ca exchange currents that developed during application of Ca were unchanged. We conclude that cationic peptides can markedly promote membrane expansion from the extracellular side by favouring the loss of anionic phospholipids from the cytoplasmic membrane leaflet.

Discussion.

It is long been known that many cell types can expand their surface membrane by a large amount in response to elevations of cytoplasmic Ca (Coorssen et al., 1996; Ninomiya et al., 1996; Kasai et al., 1999; Togo et al., 2003; Kreft et al., 2004; Bretscher, 2008; Cohen et al., 2008; Yaradanakul et al., 2008), and this expansion has been suggested to play a role in the response of cells to membrane wounding (Corrotte et al., 2015). In the accompanying article (al., XXXX) we have shown that TMEM16F initiates these responses to cytoplasmic Ca elevation. Here we have demonstrated that these membrane expansion responses are directly coupled to scrambling of anionic phospholipids, that they require occupation of the TMEM16F pore by monovalent cations, and that the underlying mechanisms of membrane expansion are substantially different from classical Ca-activated exocytosis. Membrane expansion with strong probability reflects the opening of deeply invaginating surface membrane compartments that are controlled by regulated constrictions in junctional regions close to the cell surface. We subsequently discuss evidence for these hypotheses and the potential physiological functions of this surprising new form of surface membrane remodelling.

Membrane expansion does involve bona fide membrane fusion events. Our results show a very close correlation between the opening of TMEM16f channels and the expansion of the surface membrane in Jurkat cells (Fig. 7). Indeed, the time courses of transient TMEM16F activation and membrane expansion are nearly superimposable. Although cytoplasmic monovalent cations are required for membrane expansion (Figs. 9 and 11), the actual conduction of ions through TMEM16F can be entirely dissociated from membrane expansion by changing the holding potential employed in patch clamp experiments. Accordingly, we suggest that monovalent cations are used as counter charges during the outward (and inward, Figs. 9 and 11)movement of anionic phospholipids through TMEM16F. The blockade of TMEM16F conductance and membrane expansion by spermine (Fig. 5) further underscores the idea that lipids and ions likely move through the TMEM16F channel in a concerted fashion. Most importantly, we have documented here extensively that membrane expansion caused by activation of TMEM16F can be partially or completely reversed by establishing large inward cation gradients and by membrane depolarization (Fig. 9 and 11). To the best of our understanding, these results firmly contradict the idea that membrane expansion reflects genuine membrane fusion events.

Membrane expansion reflects relaxation of membrane constrictions via PS binding proteins. The present experiments verify that a novel membrane compartment is involved in the membrane expansion that occurs in response to high cytoplasmic Ca. Specifically, it involves extended, deeply invaginating compartments that can have dimension of several microns in length and breadth (Figs. 2 and 3). Nevertheless, we cannot entirely exclude that caveolae or other smaller invaginating compartments become involved in membrane expansion activated by TMEM16F. Experiments described in the accompanying article effectively eliminate any major roles of normal recycling endosomes, endoplasmic reticulum, or lysosomes. The appearance of vesicle membrane protein, VAMP4, in the surface membrane during membrane expansion confirms a previous report (Cocucci et al., 2008) but does not add substantively to our understanding of the contents of this membrane compartments. The membrane is unusual in that it does not contain a normal set of surface membrane ion transporters or ion channels (Yaradanakul et al., 2008), and it remains to be proved that this membrane pool really plays a critical role in cell wounding.

The hypothesis that membrane expansion reflects relaxation of membrane binding proteins that constrict the necks of these compartments is supported by the following evidence: (1) Membrane expansion is reversible as expected for a direct dependence on protein binding to anionic phospholipids (Figs. 9, 11, and 13). (2) Large-scale membrane expansion can be initiated in the complete absence of cytoplasmic Ca by 'chelating' anionic phosopholipids with cationic peptides or proteins that bind strongly anionic phospholids (Fig. 12). (3) Membrane expansion can be reversed in increasing the surface membrane content of PS via application of PS/albumin complexes from the outside of the cell. (4) Membrane expansion is enhanced by incubating cells with proteins, e.g. protamine, that bind anionic phospholipids and therefore will shift the equilibrium of PS from the cytoplasmic to the extracellular surface membrane monolayer (Fig. 13).

The major open question for our working hypothesis is the identity of the membrane proteins that mediate membrane constriction, and the obvious candidates at this time include (1) dynamins (Schmid et al., 1998; Antonny et al., 2016), (2) BAR domains (McMahon and Boucrot, 2015; Suetsugu, 2016; Salzer et al., 2017), and dysferlins (Demonbreun and McNally, 2016). For now, we have no reason to favour one system over another. Each of these membrane-shaping systems could allow regulation of membrane expansion by molecular mechanisms besides phospholipid scrambling, as each of these systems is known to be regulated by factors

besides binding to anionic lipids. In this sense, loss of anionic lipids to the extracellular leaflet is just one of many mechanisms that will regulate this form of membrane expansion.

Physiological roles of exocytosis-indepednent membrane expansion. The potential physiological roles of membrane expansion without membrane fusion events includes all of the same physiological roles attributed to exocytosis. That is, this form of membrane expansion can mediate the release of cytokines and other chemical to the extracellular space, can bring new membrane proteins into the cell surface, and can expand the cell surface so as to allow cell growth and/or swelling. The surprise is simply that the existence of this form of membrane expansion was not realized until now. Expansion can occur with as little as 1 micromolar free Ca (Fig. 5), but it can also potentially occur without any requirement for Ca (Fig. 12) if the affinity of membrane binding proteins involved might be regulated. It is probable, and indeed highly likely, that many descriptions of membrane expansion in the literature, expecially electrophysiological descriptions, in fact will be attributable to the processes described here, rather than to genuine exoctic events. It remains to be tested whether such events occur in cells that do not express TMEM16F and it remains to be determined in what physiological events this unexpected form of membrane expansion plays a key role.

Acknowledgments: We thank Mei-Jung Lin for technical help and discussion. CB was supported by The Rosetrees Trust (M155), MRC Doctoral Training Grant (1132770), and the UCL Bogue Fellowship. DH and MF were supported by National Institutes of Health, USA (HL119843, T32DK007257).

Materials and Methods

Methods are essentially the same as in the accompanying article. Baby hamster kidney (BHK) cells expressing cardiac NCX1 Na/Ca exchangers were grown as described. Cells were imaged using confocal microscopy with excitation at 543 nm and emission at 580LP. Cells were patch clamped and electrical parameters monitored as described. Trypan Blue (100 µg/ml) was favoured as a membrane dye because it binds more proportionally to membrane area (Cm) than other dyes, such as FM dyes, when anionic phospholipids scramble. Fluorescent line scans of images obtained through the EZ-C1 were determined by subtracting the equivalent background fluorescence approx. Membrane fluorescence depth in microns was determined from line scan images and quantified in ImageJ using 4 distinct membrane regions per cell.

Solutions. Table 1 provides the detailed composition of major solutions employed.

	Cytoplasmic Solutions (mM)					**Extracellular Solutions (mM)**				
	#1	**#2**	**#3**	**#4**	**#5**	**#1**	**#2**	**#3**	**#4**	**#5**
Dextrose	0	0	0	0	0	10	0	0	0	0
HEPES	10	20	20	30	20	10	10	10	10	10
KOH	140	140	0	160	0	5	0	0	0	0
NaOH	5	0	40	0	20	130	0	0	0	0
CsOH	0	0	0	0	0	0	0	140	0	0
TEA-OH	0	0	20	0	120	0	20	0	140	0
NMG	0	0	80	0	0	0	120	0	0	0
EGTA	0.5	5	0.5	30	30	0	0.5	0.5	0.5	0.5
$CaCO_3$	0	0	0	20	25	0	0	0	0	0
$CaCl_2$	0.25	4.6	0.25	0	0	0	0	0	0	0
$MgCl_2$	0.5	0.5	0.5	0	0	2	4	4	4	4
Aspartate	0	125	115	90	125	0	125	125	125	0
HCl	145	0	0	0	0	135	0	0	0	0
Trehalose	0	0	0	0	0	0	0	0	0	300
Sucrose	0	0	0	0	0	0	0	0	0	0
pH	7.0	7.0	7.0	7.0	7.0	7.0	7.4	7.4	7.4	7.4

Table 1.

Reagents. Unless stated otherwise, reagents were from Sigma-Aldrich and were the highest available grade. 5µM ionomycin free acid (Calbiochem) was used unless otherwise stated.

Other reagents used were 5μM FM 4-64 (Life Technologies), 50-500μM spermine (Sigma-Aldrich), and 100μg/ml (0.01%) Trypan Blue (Sigma-Aldrich). Rhodamine-conjugated hepta-lysine (rhodamine-KKKKKKK-amide; K7) was prepared by Multiple Peptide Systems (NeoMPS, Inc.).

Simulation of TMEM16F function and deep membrane compartments (Figs. 8 and 10). The simulations were written in Matlab. In the initial state, all PS (PS_{tot}, 100 units) is assumed to be cytoplasmic:

(1) PS_i=100, and PS in the outer monolayer (PS_o) is

(2) $PS_o=PS_{tot}-PS_i$

At any time, the fraction of active TMEM16F channels (F_{active}, see Fig. 1B) is dependent on Ca binding to a single TMEM16F site with a K_{50} of 20 μM. In addition, it is assumed that TMEM16F channels require binding of two PS molecules at regulatory sites with a K_{50} of 120 PS units and a Hill slope of 2 to become active (see Fig. 1B). Thus, the fraction of active TMEM16 channels (F_{active}) is:

(3) $F_{act}=Ca_i/(Ca_i+20\mu M) \bullet PSi^2/(PSi^2+120\ PSi\ units^2)$

The active state (F_{active}) is then subdivided into conducting channels that have no PS bound within their open pores (E_o), channels that have one PS bound within the pore on the cytoplasmic side (E_1), and that have one PS bound within the pore on the extracellular side (E_2). For simplicity, we ignore the possibility of channels having dual PS occupancy.

The rates of PS translocation in TMEM16F (K_{PSX}), PS binding by TMEM16F (K_{PSon}) and dissociation from TMEM16F (K_{PSoff}) are assigned as follows, relevant to the total PS population of 100:

(4) $K_{PSx}=20\ s^{-1}$

(5) $K_{PSon}=75\ PS^{-1}\bullet s^{-1}$;

(6) $K_{PSoff}=400\ s^{-1}$

To simulate ion translocation within the E_0 state of the F_{active} fraction of TMEM16F (cation permeation model in Fig. 1), a two-site model was employed with the rates of ion binding (K_{on}), dissociation (K_{off}), and translocation between occupancy sites (K_x) relativized to a translocation rate (K_x) of 1 s^{-1}. K_{on} is 0.2 $mM^{-1}s^{-1}$ and K_{off} was 5 s^{-1}. When changes of membrane potential (Em) were simulated, K_x was modified by a single, symetrical barrier function,

(7) $K_{em} = e^{(0.5 \cdot Em/26mV)}$.

With internal (X_i) and external (X_o) cation concentrations in mM, calculation of TMEM16F ion occupancy states and permeation rates proceed as follows (see Fig. 1B):

(8) $K_1=N_o \bullet K_{on}$

(9) $K_2=K_{off}$

(10) $K_3= K_{off}$

(11) $K_4=Ni \bullet K_{on}$

(12) $K_5= K_{off}$

(13) $K_6=No \bullet K_{on}$

(14) $K_7=Ni \bullet K_{on}$

(15) $K_8= K_{off}$

(16) $K_9=K_x \bullet K_{em}$

(17) $K_{10}=K_x/K_{em}$

Using a King-Altman procedure (Lam and Priest, 1972) to calculate occupancy of the four permeation states,

(18) $X_1=K_2 \bullet K_4 \bullet (K_7+K_6)+K_5 \bullet K_7 \bullet (K_2+K_3)+K_{10} \bullet (K_2+K_3) \bullet (K_7+K_6)$

(19) $X_2=K_1 \bullet K_7 \bullet (K_4+K_5)+K_4 \bullet K_6 \bullet (K_1+K_8)+(K_{10} \bullet K_1+K_9 \bullet K_4) \bullet (K_7+K_6)$

(20) $X_3=K_1 \bullet K_3 \bullet (K_7+K_6)+K_8 \bullet K_6 \bullet (K_2+K_3)+K_9 \bullet (K_6+K_7) \bullet (K_3+K_2)$

(21) $X_4=K_2 \bullet K_8 \bullet (K_4+K_5)+K_3 \bullet K_5 \bullet (K_1+K_8)+(K_9.K_5+K_{10} \bullet K_8) \bullet (K_3+K_2)$

With $S=X_1+X_2+X_3+X_4$,

The fractional occupancies of the four states are then

(22) $F_1=X_1/S$, $F_2=X_2/S$, $F_3=X_3/S$ and $F_4=X_4/S$, where F_1 is occupied on the cytoplasmic side by 1 cation, F_2 by twocations, F_3 by a cation on the extracellular side, and F_4 is unoccupied. The (relative) permeation rate (R_{net}) is then:

(23) $Rnet=F_3 \bullet K_{10}-F_1 \bullet K_9$

Next, the active TMEM16F states with PS bound to the inner (E_1) and outer (E_2) pore binding sites are integrated over time. Assuming that PS can bind from the cytoplasmic side to all E_0 states with cations occupying the cytoplasmic site (i.e. F1 + F2 states), assigning K_{pson} (75 $PS^{-1} \bullet s^{-1}$) to be the second order rate of PS binding, K_{psoff} to be the PS dissociation rate from E1 states (400 s^{-1}), and K_{psx} (20 s^{-1})to be the PS translocation rate between PS sites in the pore, we have:

(26) $dE_1/dt= [PS_i \bullet E_0 \bullet F_{act} \bullet K_{PSON} \bullet (F_1+F_2)-E_1 \bullet K_{PSOFF}]+(E_2-E_1) \bullet K_{PSX}$.

To simulate the expectation that lipids in the outer monolayer are more ordered and less fluid, we assume that K_{PSON} is two-fold slower and that K_{PSOFF} is two-fold faster on the extracellular side:

(27) $dE_2/dt= [PS_o \bullet E_0 \bullet Fact \bullet K_{PSON} * (F_3+F_2)/2 - E_2 * K_{PSOFF} \bullet 2] + (E_1-E_2) \bullet K_{PSX}$.

The fraction of active channels without PS bound with the pore region is calculated:

(28) $E_0=1-E_1-E_2$,

PS changes in the cytoplasmic leaflet (PS_i) are integrate,:

(29) $dPS_i/dt = E1 \bullet K_{PSOFF} - PS_i \bullet E_0 \bullet K_{PSON} \bullet F_{act} \bullet (F_1 + F_2)$,

PS in the extracellular leaflet is calculated=,

(30) $PS_o=PS_{tot}-PS_{i,}$

the relative TMEM16F current is calculated,

(31) $I_{TMEM16F}=R_{net} \bullet F_{active} \bullet E_0$,

and finally, the fraction of deep membrane compartments open to the extracellular space is calculated. We assume here that compartment opening depends on the binding of 4 PS molecules with a K_{50} of somewhat less than one-half of the total PS in the inner monolayer:

(32) $F_{open}=35^4/(PS_i^4+35^4)$.

Simulations were carried out with accuracy checks to insure that simulation error was less that the width of lines in the simulated results presented.

Figure Legends.

Figure 1. Working hypotheses to account for TMEM16F-mediated membrane expansion in Jurkat and BHK cells**.** **(A)** The membrane compartments that expand the cell surface extend deeply into cells and are closed by proteins that bind anionic phospholipids. Loss of anionic phospholipids from the cytoplasmic leaflet relaxes the constrictions and opens the compartments to the extracellular space. **(B)** TMEM16F channels are closed in the absence of cytoplasmic Ca. When cytoplasmic Ca rises, TMEM16f channels bind Ca and open with a nearly linear dependence on Ca concentration. Anionic phospholipids can enter TMEM16f channels (see expanded diagram) only when a cation is bound within the channel near the pore opening. Anionic phospholipids permeate the channel together with monovalent cations in an electroneutral fashion. Accordingly, cation gradients can influence the direction of movement of anionic phospholipids. TMEM16F channels enter an inactive state when PS is lost from cytoplasmic binding sites.

Figure 2. Ionomycin-induced membrane expansion involves a membrane compartment that extends deeply into Jurkat, HEK293, and BHK cells. **(A)** Reversible trypan blue (TB, 100 µg/ml) staining of BHK cells was determined before and after application ionomycin in WT and TMEM16F null Jurkat T-cells. Changes of TB fluorescence (%) are plotted against changes of C_m (%) caused by ionomycin treatment. Linear regression of results with 95% C.I. confirms a linear correlation between TB fluorescence and membrane area (C_m) (PCC=0.9). Images **(B)** and fluorescent line scans **(C)** during application of 100 µg/ml TB in Jurkat WT and null cells before (blue) and after (red) ionomycin-induced exocytosis. Scale bars are 5µm. Average membrane fluorescence depth and SEM quantified from **B** for cell lines with and without TMEM16F expression. (**$p \leq 0.01$) in Jurkat **(D)** and HIK293 **(E)** cells. Mean values with SEM are given with n>4. (F) Confocal imaging a representative BHK cell, with and without TB application, before and after activation of constitutively expressed NCX1 Na/Ca exchangers by 4 mM extracellular Ca with 40 mM cytoplasmic Na. The membrane compartments that expand the cell surface extend several microns into the cell and converge to a "neck"-like structure at the interface to the peripheral membrane surface.

Figure 3. Membrane expansion follows closely the exposure of anionic phospholipids, as monitored by binding of heptalysine-rhodamine (K7r). Similar to other membrane probes, K7r reveals the opening of deeply invaginating membrane compartments during membrane

expansion. Here and in all subsequent figures, concentrations are given in millimolar unless indicated otherwise.

Figure 4. Analysis of VAMP protein appearance in the surface membrane during membrane expansion. Among VAMP2-, VAMP4- and VAMP7- GFP fusion proteins, VAMP4 fusions preferentially enter into the cell surface during membrane expansion. Fluorescence recordings in a BHK cell constitutively expressing NCX Na/Ca exchangers and transfected to express VAMP4-pHluorin (pHL) fusion protein. Activation of Ca influx via NCX1 caused a 60% expansion of the surface membrane and a 55% increase of TB fluorescence. VAMP-PHL fusion protein accessible to the extracellular space, determined by the quench of VAMP-pHL fluorescence that occurs on application of TB, is negligible in the control state and increases to 25% of the total VAMP-pHL fluorescence after membrane expansion.

Figure 5. TMEM16F-mediated membrane expansion can occur profusely with 1 to 3 μM free cytoplasmic Ca, albeit slowly. **(A)** In BHK cells, membrane area (Cm) increases by 40% over 10 min when cells are perfused with solutions containing 1 μM free Ca, buffered with 30 mM EGTA. Membrane expansion does not occur in the absence of Ca, and membrane expansion is blocked by spermine (1 mM), as expected from studies in Jurkat cells. **(B)** In Jukat cells, 3 μM free Ca is required to elicit robust membrane expansion that amounts to 25% of membrane area over 10 min. Membrane area decreases by 10% over 10 min in the absence of Ca, and in TMEM16F null cells membrane area decreases by 35% in the presence of 3 μM free Ca.

Figure 6. Reversal of membrane expansion by removal of extracellular ions. Membrane compartments that expand the surface membrane during Ca influx in BHK cells can be closed by substitution of extracellular monovalent ions by trehalose. **(A)** Ca influx results in a 75% increase of C_m on average in these BHK cells (n=6), and application of trehalose within 30 s of the expansion response reverses the membrane expansion by 86% on average. The reversal of membrane expansion remains stable upon removal of trehalose and reapplication of standard extracellular solution. (B) Plot of all 9 experimental results to illustrate that the extended surface membrane compartments reopen if the membrane expansion responses are small, while the compartments remain closed after trehalose if the membrane expansion responses are large.

Figure 7. Relationships between membrane conductance (G_m), current (I_m) and capacitance (C_m) during ionomycin induced membrane expansion in Jurkat T cells. **(A)** Using standard experimental solutions with WT Jurkat T cells, G_m and I_m have similar time courses (lower recordings), and the integral of G_m, $\int G_m$, tracks the time course of membrane expansion (ΔC_m)

(upper recordings) during application of ionomycin (5 μM). Records were scaled to start and end at the same points, n >10. **(B))** Percentage change in C_m 30s after ionomycin treatment of WT Jurkat cells. Cells were perfused with indicated cytoplasmic solutions for >200s before ionomycin treatment. Extracellular (OUT) and cytoplasmic (IN) solutions were as shown: Standard cytoplasmic (KCl), Sodium Aspartate (NaAs), Potassium Aspartate (KAs), NMG Aspartate (NmAs), Ringer solution (NaCl), and isotonic sucrose (Suc) with 0.5 mM EGTA with 4 mM (OUT) or 0.5 mM $MgCl_2$ (IN). **(C and D)** Ion permeation does not influence membrane expansion. Solutions were symmetrical NmAs with 30 mM NMG replaced by 30 mM Na on the cytoplasmic side to generate outward Na current. Membrane potential was held at +50 or – 50 mV during the entire experiments. Representative recordings are shown in **C**; mean values and SEM for n>7 at each potential are shown in **D.** Ionomycin treatment transiently increases conductance (blue) and generates outward Na current (green) at +50 mV but not at -50 mV. However, C_m (red) increases to the same extent and at the same maximal rate at -50 and +50 mV.

Figure 8. Simulation of TMEM16F function and membrane expansion accompanying TMEM16F activation. (A) Predicted results for activation of TMEM16F by increasing cytoplasmic free Ca from 0 to 20 μM. Nearly all subsurface membrane compartments open to the extracellular space, TMEM16F current inactivates by about 90%, and about 80% of PS translocates from the cytoplasmic leaflet to the extracellular membrane leaflet. (B) Membrane expansion induced by140 mM extracellular Cs when cytoplasmic solutions contain TEA and 20 mM Na. Responses 1 to 4 were generated by substituting extracellular Cs for TEA at progressively later time points. When membrane expansion is allowed to come to nearly steady state, membrane expansion reverses by 25% when TEA is replaced by Cs in the extracellular solution.

Figure 9. Experimental results verifying the predictions of simulations presented in Fig. 7 (i.e. with only 20 mM Na on the cytoplasmic side with 120 mM TEA). (A) Blockade of membrane expansion by substituting extracellular TEA for Na. (B) Partial reversal of membrane expansion by substituting extracellular TEA for Na. (C) Blockade and partial reversal of membrane expansion by substituting extracellular TEA for Cs. (D) Documentation of the rapidity with which membrane area changes can be directed by changing ion gradients. Cs induces reversal of membrane expansion, and TEA induces renewed membrane expansion within just a few seconds upon changing solutions.

Figure 10. Simulation of effects of membrane potential on membrane expansion in the presence of 140 mM cytoplasmic TEA and either 140 mM TEA or Cs on the cytoplasmic side. The cytoplasmic is simulated to contain 3 μM free Ca. (A) Extracellular TEA (140 mM) is substituted for Cs at 3 different membrane potentials (-60, 0 and +60 mV). Hyperpolarization promotes membrane expansion, depolarization prevents membrane expansion. (B) Depolarization reversibly causes closure of the deeply extended surface membrane compartments, while hyperpolarization causes opening of the compartments under the condition of imposed inward cation gradients.

Figure 11. Activation of membrane expansion by extracellular Cs and by hyperpolarization. **(A)** With TEA on both membrane sides membrane expansion and scrambling are negligible in the presence of 5 μM free cytoplasmic Ca. Substitution of extracellular TEA for Cs activates both anionic phosopholipid exposure and membrane expansion (up to 65%) in parallel. **(B)** Membrane expansion with 5 μM free Ca (~45% expansion; 140 mM cytoplasmic TEA) reverses almost completely within 1 min when membrane potential is depolarized by 50 mV. The membrane expansion develops again rapidly when membrane potential is hyperpolarized to -50 mV.

Figure 12. Peptides (heptalysine-rhodamine, K7r) and proteins (protamine) that bind anionic phospholipids cause immediate membrane expansion when included in pipette solutions in the absence of Ca and the presence of 10 mM EGTA. **(A)** BHK cells increase membrane area by 29.7% on average when opened in the cytoplasmic presence of 3 mg/ml protamine. **(B)** BHK cells increase membrane area on average by 37.1 % when opened in the presence of 0.2 mM K7. **(C)** Jurkat cells increase their membrane area by 40.1% on average when opened in ther presence of 3 mg/ml protamine.

Figure 13. Reversal of membrane expansion by extracellular PS-albumin complexes and enhancement of membrane expansion by extracellular PS-binding peptides/proteins. **(A)** Membrane expansion in the presence of 3 μM free cytoplasmic Ca can be reversed by application of extracellular PS-albumin complexes (120 μM). **(B)** Membrane expansion by activation of reverse Na/Ca exchange current in BHK cells can be doubled by including cationic proteins that bind PS (protamine, 3 mg/ml) in extracellular solutions.

Reference List

al., B.e. XXXX. TMEM16F activation by Ca2+ triggers surface membrane expansion and directs Programmed Death receptor (PD-1) trafficking. . *eLife*. xx:xxx-xxx.

Antonny, B., C. Burd, P. De Camilli, E. Chen, O. Daumke, K. Faelber, M. Ford, V.A. Frolov, A. Frost, J.E. Hinshaw, T. Kirchhausen, M.M. Kozlov, M. Lenz, H.H. Low, H. McMahon, C. Merrifield, T.D. Pollard, P.J. Robinson, A. Roux, and S. Schmid. 2016. Membrane fission by dynamin: what we know and what we need to know. *The EMBO journal*. 35:2270-2284. doi:10.15252/embj.201694613.

Bartholow, L.C., and R.P. Geyer. 1982. Influence of phospholipid structure on sterol efflux induced by albumin-phospholipid complexes. *Biochemistry*. 21:1271-1273.

Bretscher, M.S. 2008. Exocytosis provides the membrane for protrusion, at least in migrating fibroblasts. *Nature reviews. Molecular cell biology*. 9:916. doi:10.1038/nrm2419-c3.

Cocucci, E., G. Racchetti, P. Podini, and J. Meldolesi. 2007. Enlargeosome traffic: exocytosis triggered by various signals is followed by endocytosis, membrane shedding or both. *Traffic (Copenhagen, Denmark)*. 8:742-757. doi:10.1111/j.1600-0854.2007.00566.x.

Cocucci, E., G. Racchetti, M. Rupnik, and J. Meldolesi. 2008. The regulated exocytosis of enlargeosomes is mediated by a SNARE machinery that includes VAMP4. *Journal of cell science*. 121:2983-2991. doi:10.1242/jcs.032029.

Cohen, R., B.M. Schmitt, and D. Atlas. 2008. Reconstitution of depolarization and Ca2+-evoked secretion in Xenopus oocytes monitored by membrane capacitance. *Methods in molecular biology (Clifton, N.J.)*. 440:269-282. doi:10.1007/978-1-59745-178-9_21.

Cooper, S.T., and P.L. McNeil. 2015. Membrane Repair: Mechanisms and Pathophysiology. *Physiological reviews*. 95:1205-1240. doi:10.1152/physrev.00037.2014.

Coorssen, J.R., H. Schmitt, and W. Almers. 1996. Ca2+ triggers massive exocytosis in Chinese hamster ovary cells. *The EMBO journal*. 15:3787-3791.

Corrotte, M., T. Castro-Gomes, A.B. Koushik, and N.W. Andrews. 2015. Approaches for plasma membrane wounding and assessment of lysosome-mediated repair responses. *Methods in cell biology*. 126:139-158. doi:10.1016/bs.mcb.2014.11.009.

Demonbreun, A.R., and E.M. McNally. 2016. Plasma Membrane Repair in Health and Disease. *Current topics in membranes*. 77:67-96. doi:10.1016/bs.ctm.2015.10.006.

Fujii, T., A. Sakata, S. Nishimura, K. Eto, and S. Nagata. 2015. TMEM16F is required for phosphatidylserine exposure and microparticle release in activated mouse platelets. *Proceedings of the National Academy of Sciences of the United States of America*. 112:12800-12805. doi:10.1073/pnas.1516594112.

Groulx, N., F. Boudreault, S.N. Orlov, and R. Grygorczyk. 2006. Membrane reserves and hypotonic cell swelling. *The Journal of membrane biology*. 214:43-56. doi:10.1007/s00232-006-0080-8.

Harrisson, F., M. Callebaut, and L. Vakaet. 1981. Microspectrographic analysis of trypan blue-induced fluorescence in oocytes of the Japanese quail. *Histochemistry*. 72:563-578.

Kasai, H., T. Kishimoto, T.T. Liu, Y. Miyashita, P. Podini, F. Grohovaz, and J. Meldolesi. 1999. Multiple and diverse forms of regulated exocytosis in wild-type and defective PC12 cells. *Proceedings of the National Academy of Sciences of the United States of America*. 96:945-949.

Kreft, M., M. Stenovec, M. Rupnik, S. Grilc, M. Krzan, M. Potokar, T. Pangrsic, P.G. Haydon, and R. Zorec. 2004. Properties of Ca(2+)-dependent exocytosis in cultured astrocytes. *Glia*. 46:437-445. doi:10.1002/glia.20018.

Lam, C.F., and D.G. Priest. 1972. Enzyme kinetics. Systematic generation of valid King-Altman patterns. *Biophysical journal*. 12:248-256. doi:10.1016/s0006-3495(72)86084-3.

McMahon, H.T., and E. Boucrot. 2015. Membrane curvature at a glance. *Journal of cell science*. 128:1065-1070. doi:10.1242/jcs.114454.

Moe, A.M., A.E. Golding, and W.M. Bement. 2015. Cell healing: Calcium, repair and regeneration. *Seminars in cell & developmental biology*. 45:18-23. doi:10.1016/j.semcdb.2015.09.026.

Ninomiya, Y., T. Kishimoto, Y. Miyashita, and H. Kasai. 1996. Ca2+-dependent exocytotic pathways in Chinese hamster ovary fibroblasts revealed by a caged-Ca2+ compound. *The Journal of biological chemistry*. 271:17751-17754.

Racchetti, G., R. D'Alessandro, and J. Meldolesi. 2012. Astrocyte stellation, a process dependent on Rac1 is sustained by the regulated exocytosis of enlargeosomes. *Glia*. 60:465-475. doi:10.1002/glia.22280.

Salzer, U., J. Kostan, and K. Djinovic-Carugo. 2017. Deciphering the BAR code of membrane modulators. *Cellular and molecular life sciences : CMLS*. 74:2413-2438. doi:10.1007/s00018-017-2478-0.

Schmid, S.L., M.A. McNiven, and P. De Camilli. 1998. Dynamin and its partners: a progress report. *Current opinion in cell biology*. 10:504-512.

Scudieri, P., E. Caci, A. Venturini, E. Sondo, G. Pianigiani, C. Marchetti, R. Ravazzolo, F. Pagani, and L.J. Galietta. 2015. Ion channel and lipid scramblase activity associated with expression of TMEM16F/ANO6 isoforms. *The Journal of physiology*. 593:3829-3848. doi:10.1113/jp270691.

Shaul, P.W., and R.G. Anderson. 1998. Role of plasmalemmal caveolae in signal transduction. *The American journal of physiology*. 275:L843-851.

Sudhof, T.C., and J.E. Rothman. 2009. Membrane fusion: grappling with SNARE and SM proteins. *Science (New York, N.Y.)*. 323:474-477. doi:10.1126/science.1161748.

Suetsugu, S. 2016. Higher-order assemblies of BAR domain proteins for shaping membranes. *Microscopy (Oxford, England)*. 65:201-210. doi:10.1093/jmicro/dfw002.

Suzuki, J., T. Fujii, T. Imao, K. Ishihara, H. Kuba, and S. Nagata. 2013. Calcium-dependent phospholipid scramblase activity of TMEM16 protein family members. *The Journal of biological chemistry*. 288:13305-13316. doi:10.1074/jbc.M113.457937.

Togo, T., J.M. Alderton, and R.A. Steinhardt. 2003. Long-term potentiation of exocytosis and cell membrane repair in fibroblasts. *Molecular biology of the cell*. 14:93-106. doi:10.1091/mbc.E02-01-0056.

Tojima, T., R. Itofusa, and H. Kamiguchi. 2014. Steering neuronal growth cones by shifting the imbalance between exocytosis and endocytosis. *The Journal of neuroscience : the official journal of the Society for Neuroscience*. 34:7165-7178. doi:10.1523/jneurosci.5261-13.2014.

van den Bogaart, G., N. Hermans, V. Krasnikov, A.H. de Vries, and B. Poolman. 2007. On the decrease in lateral mobility of phospholipids by sugars. *Biophysical journal*. 92:1598-1605. doi:10.1529/biophysj.106.096461.

Wang, T.M., and D.W. Hilgemann. 2008. Ca-dependent nonsecretory vesicle fusion in a secretory cell. *The Journal of general physiology*. 132:51-65. doi:10.1085/jgp.200709950.

Yang, H., A. Kim, T. David, D. Palmer, T. Jin, J. Tien, F. Huang, T. Cheng, S.R. Coughlin, Y.N. Jan, and L.Y. Jan. 2012. TMEM16F forms a Ca2+-activated cation channel required for lipid scrambling in platelets during blood coagulation. *Cell*. 151:111-122. doi:10.1016/j.cell.2012.07.036.

Yaradanakul, A., T.M. Wang, V. Lariccia, M.J. Lin, C. Shen, X. Liu, and D.W. Hilgemann. 2008. Massive Ca-induced membrane fusion and phospholipid changes triggered by reverse Na/Ca exchange in BHK fibroblasts. *The Journal of general physiology*. 132:29-50. doi:10.1085/jgp.200709865.

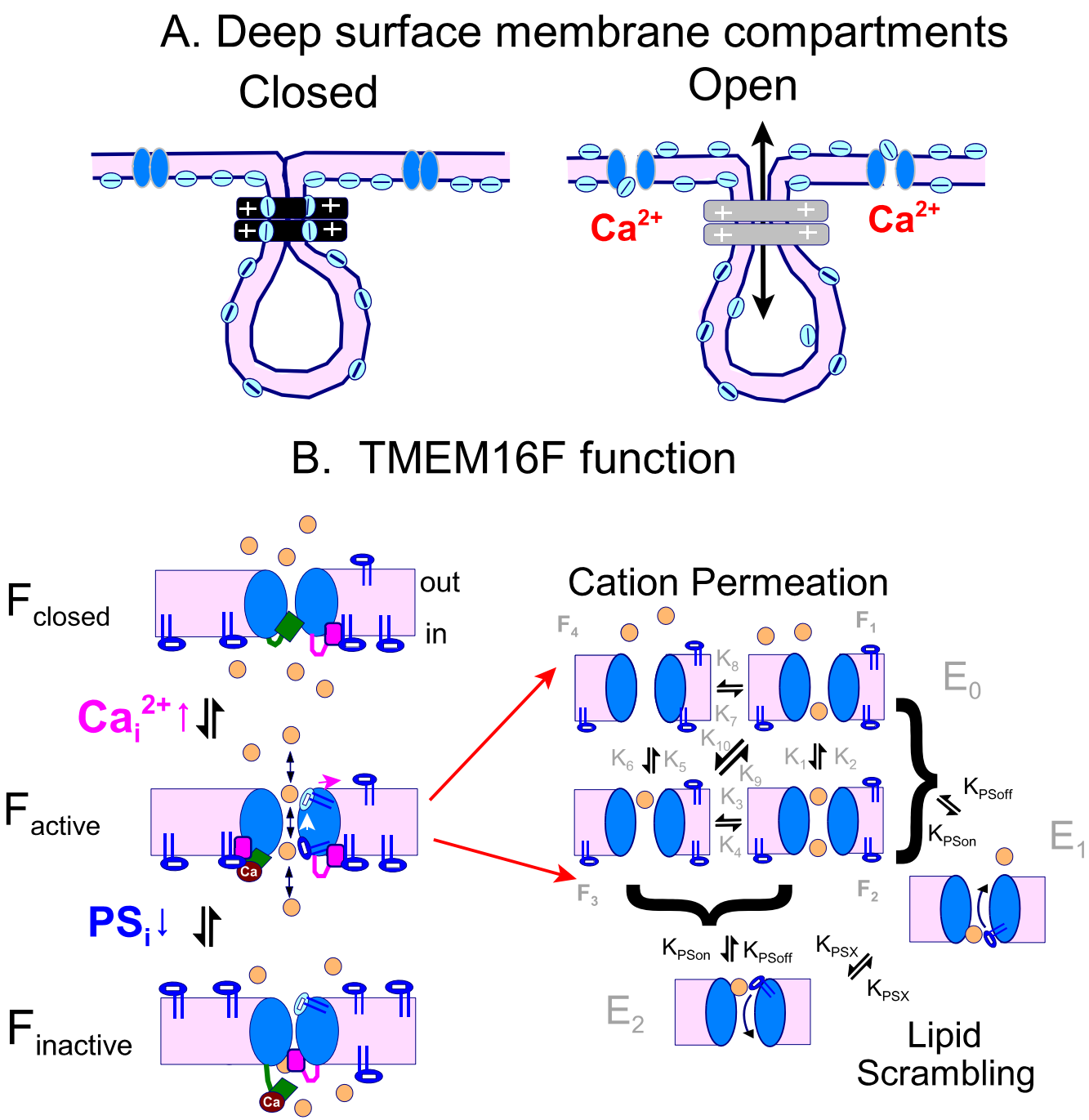
A. Deep surface membrane compartments
Closed
Open
Ca2+
Ca2+
B. TMEM16F function
F closed
out
in
Cai2+ ↑
F active
Ca
PSi ↓
F inactive
Ca
Cation Permeation
F4
F1
K8
K7
K10
K6
K5
K1
K2
K9
K3
K4
F3
F2
E0
KPSoff
KPSon
E1
KPSon
KPSoff
KPSX
KPSX
E2
Lipid
Scrambling

Fig. 1

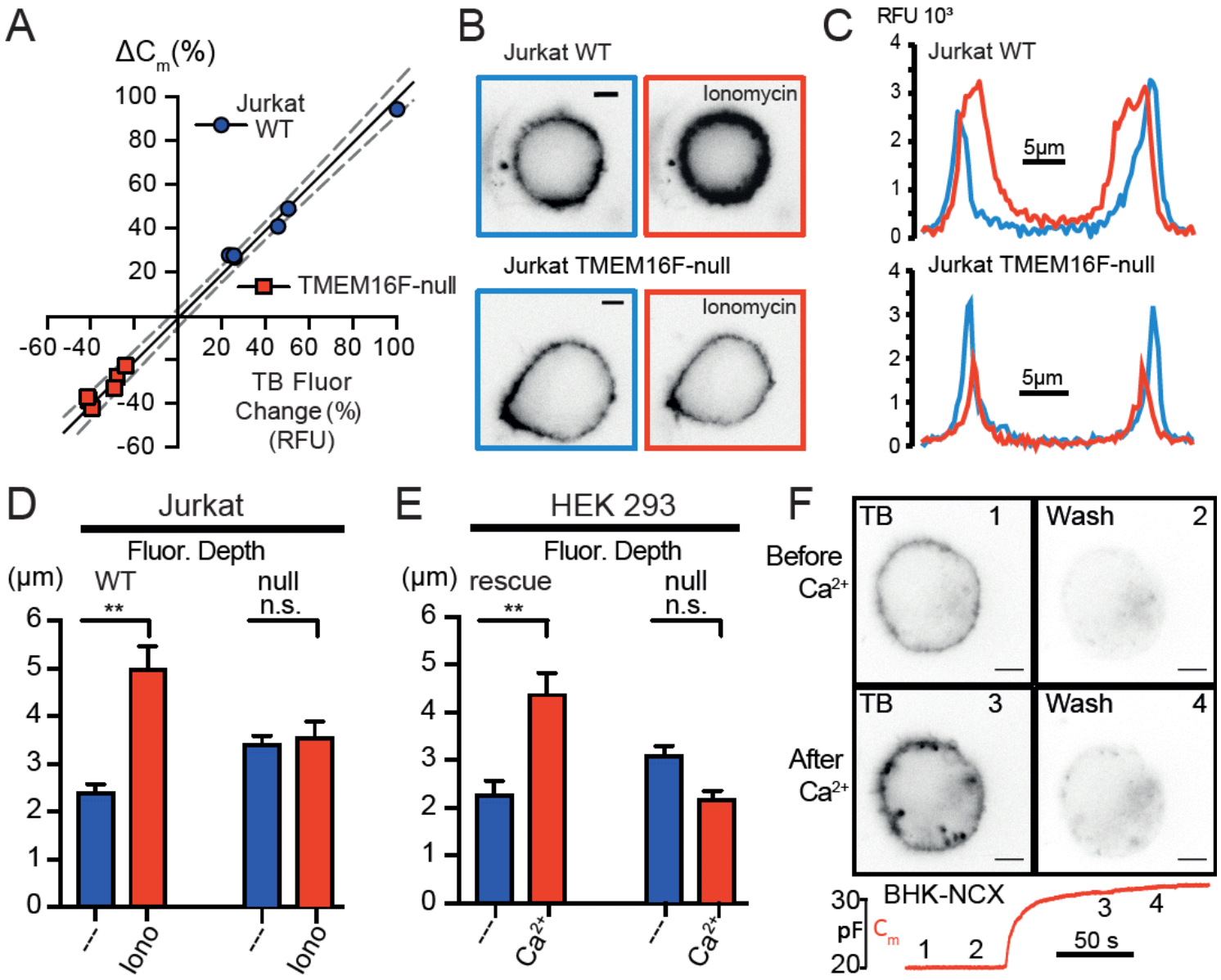
A
ΔCm(%)
Jurkat WT
TMEM16F-null
TB Fluor Change (%) (RFU)
B
Jurkat WT
Ionomycin
Jurkat TMEM16F-null
Ionomycin
C
RFU 10³
Jurkat WT
5μm
Jurkat TMEM16F-null
5μm
D
Jurkat
Fluor. Depth (μm)
WT
null
n.s.
Iono
E
HEK 293
Fluor. Depth (μm)
rescue
null
n.s.
Ca2+
F
Before Ca2+
After Ca2+
TB
Wash
BHK-NCX
Cm
pF
50 s

Fig. 2

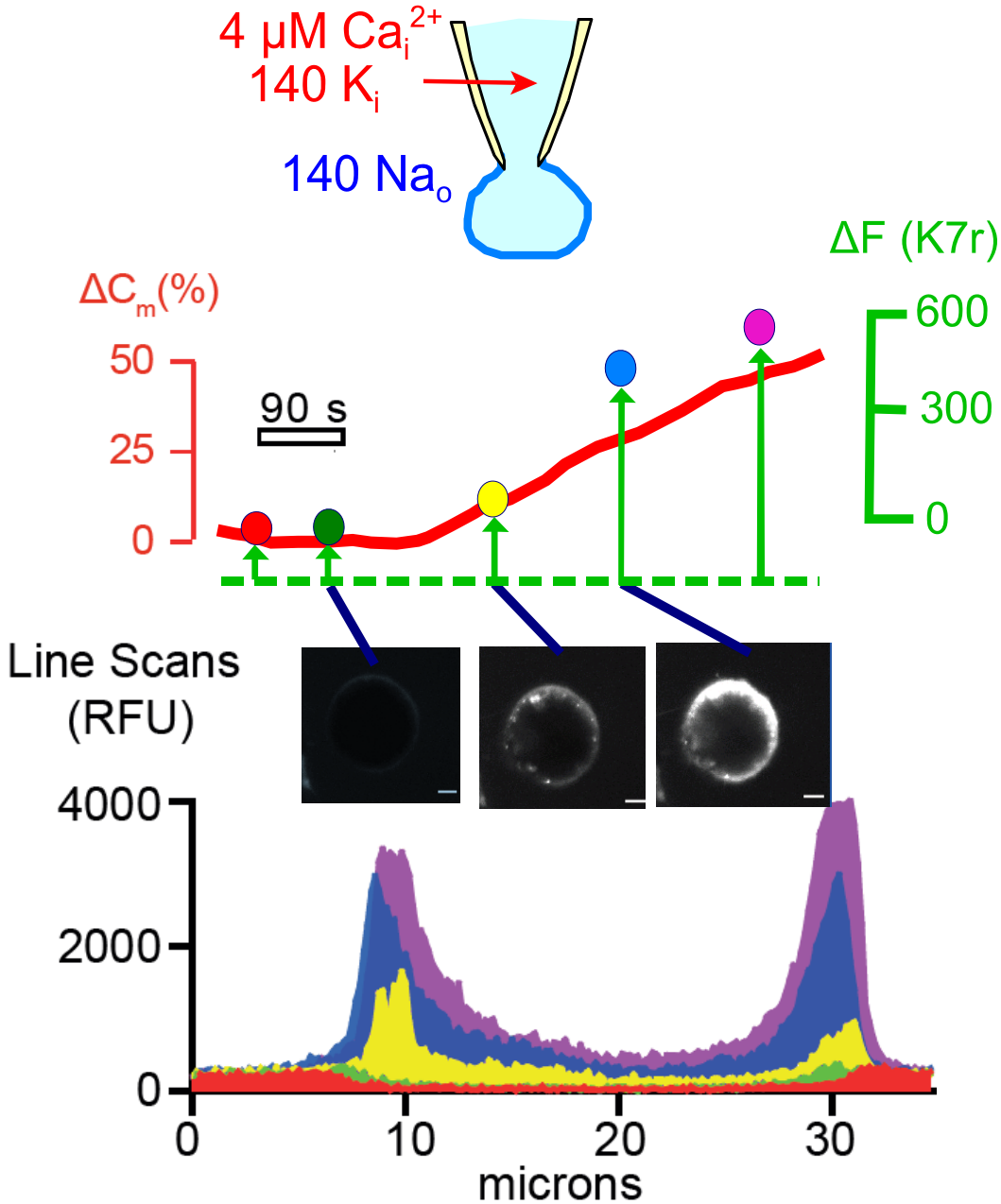
4 μM Ca_i^{2+}
140 K_i
140 Na_o
ΔF (K7r)
ΔC_m(%)
50
25
0
90 s
600
300
0
Line Scans
(RFU)
4000
2000
0
0
10
20
30
microns

Fig. 3

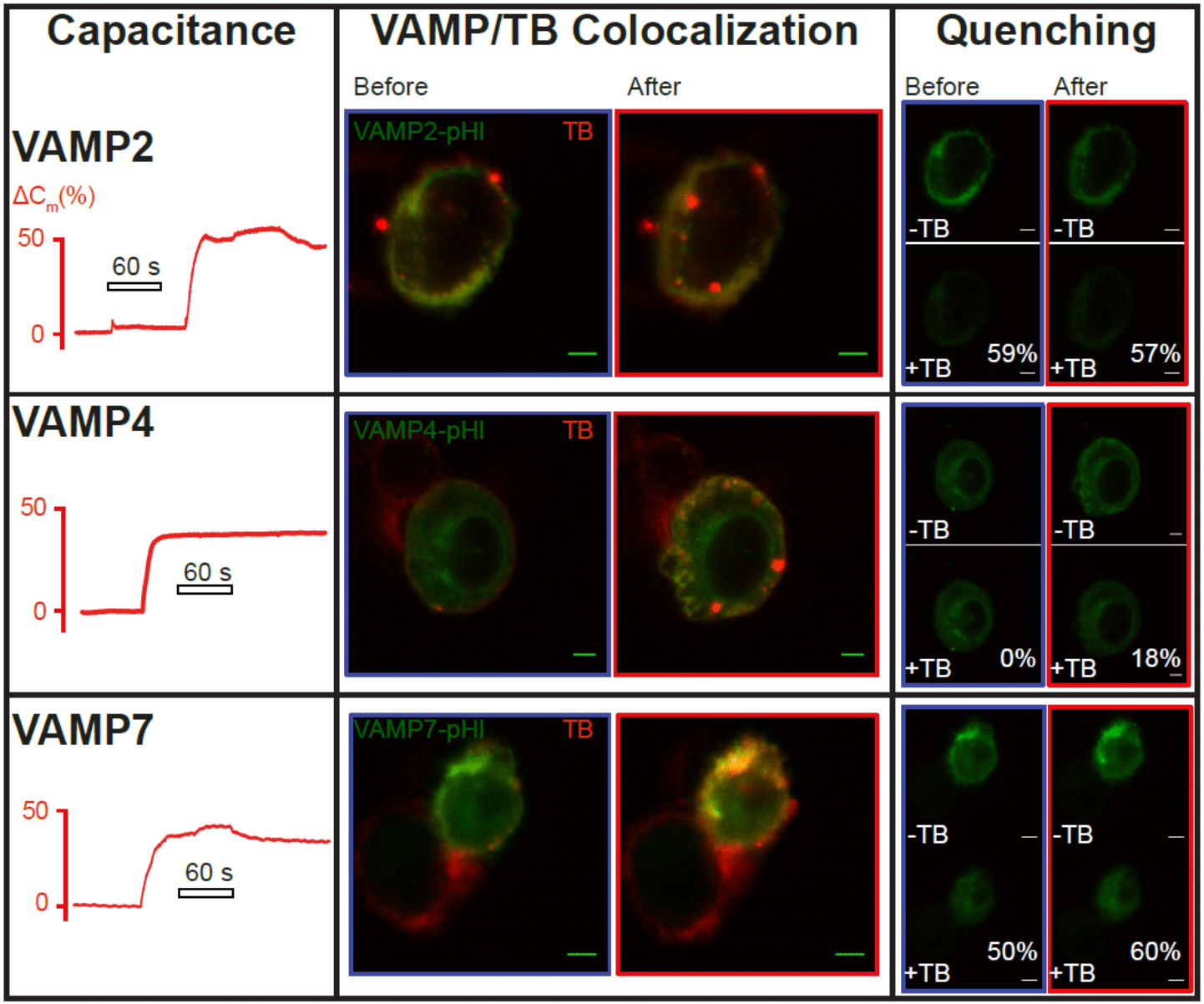
Capacitance
VAMP/TB Colocalization
Quenching
Before
After
Before
After
VAMP2
ΔCm(%)
50
0
60 s
VAMP2-pHI
TB
-TB
+TB
59%
57%
VAMP4
50
0
60 s
VAMP4-pHI
TB
-TB
+TB
0%
18%
VAMP7
50
0
60 s
VAMP7-pHI
TB
-TB
+TB
50%
60%

Fig. 4

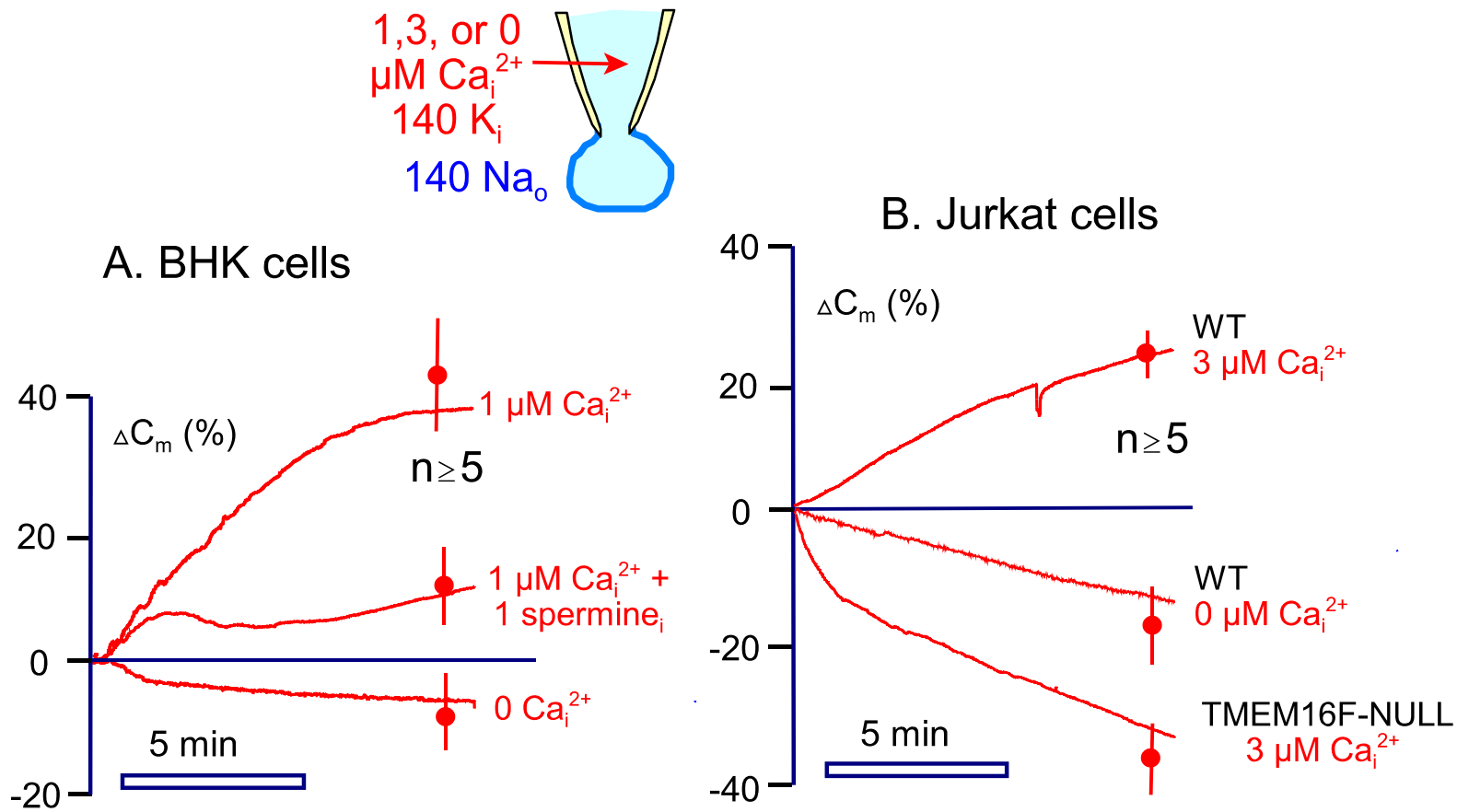
1,3, or 0
μM Ca$_i^{2+}$
140 K$_i$
140 Na$_o$
A. BHK cells
40
20
0
-20
ΔC$_m$ (%)
1 μM Ca$_i^{2+}$
n≥5
1 μM Ca$_i^{2+}$ +
1 spermine$_i$
0 Ca$_i^{2+}$
5 min
B. Jurkat cells
40
20
0
-20
-40
ΔC$_m$ (%)
WT
3 μM Ca$_i^{2+}$
n≥5
WT
0 μM Ca$_i^{2+}$
TMEM16F-NULL
3 μM Ca$_i^{2+}$
5 min

Fig. 5

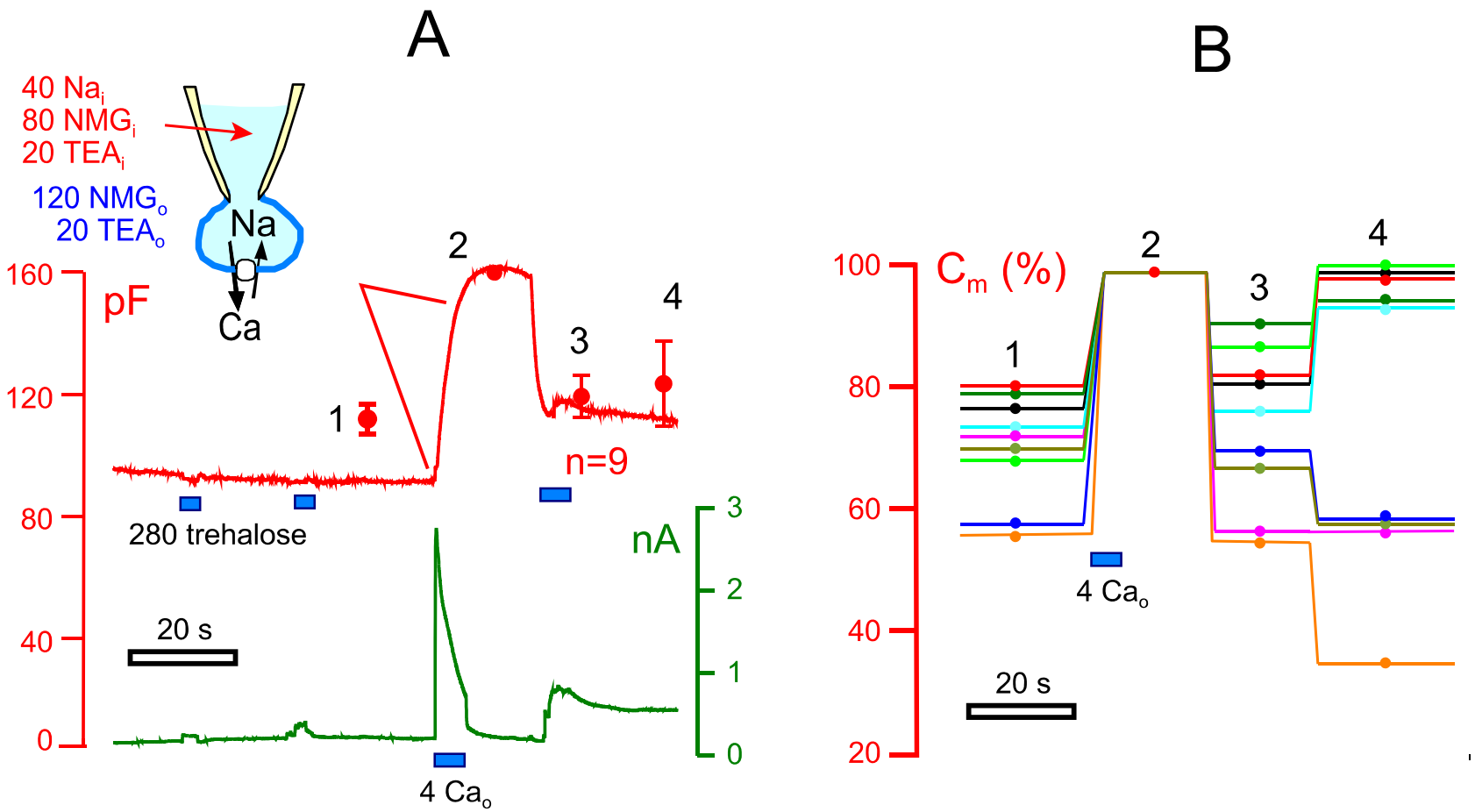
A
B
40 Na$_i$
80 NMG$_i$
20 TEA$_i$
120 NMG$_o$
20 TEA$_o$
Na
Ca
160
120
80
40
0
pF
1
2
3
4
n=9
280 trehalose
20 s
nA
3
2
1
0
4 Ca$_o$
100
80
60
40
20
C$_m$ (%)
1
2
3
4
4 Ca$_o$
20 s

Fig. 6

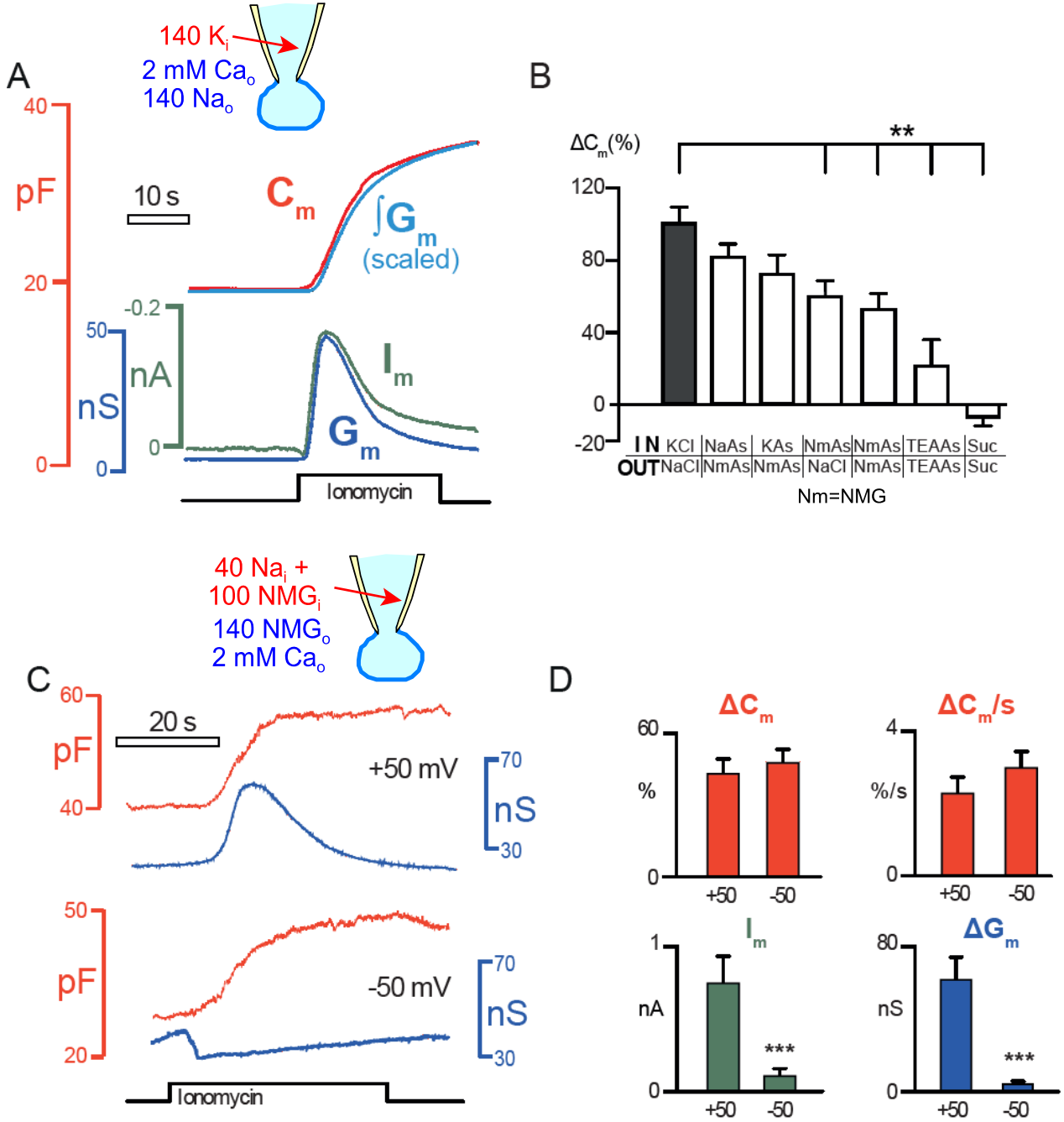
A
140 Ki
2 mM Cao
140 Nao
40
pF
20
0
10 s
Cm
∫Gm
(scaled)
-0.2
50
nA
nS
0
0
Im
Gm
Ionomycin
B
ΔCm(%)
**
120
80
40
0
-20
IN KCl NaAs KAs NmAs NmAs TEAAs Suc
OUT NaCl NmAs NmAs NaCl NmAs TEAAs Suc
Nm=NMG
C
40 Nai +
100 NMGi
140 NMGo
2 mM Cao
60
pF
40
20 s
+50 mV
70
nS
30
50
pF
20
-50 mV
70
nS
30
Ionomycin
D
ΔCm
60
%
0
+50
-50
ΔCm/s
4
%/s
0
+50
-50
Im
1
nA
0
***
+50
-50
ΔGm
80
nS
0
***
+50
-50

Fig. 7

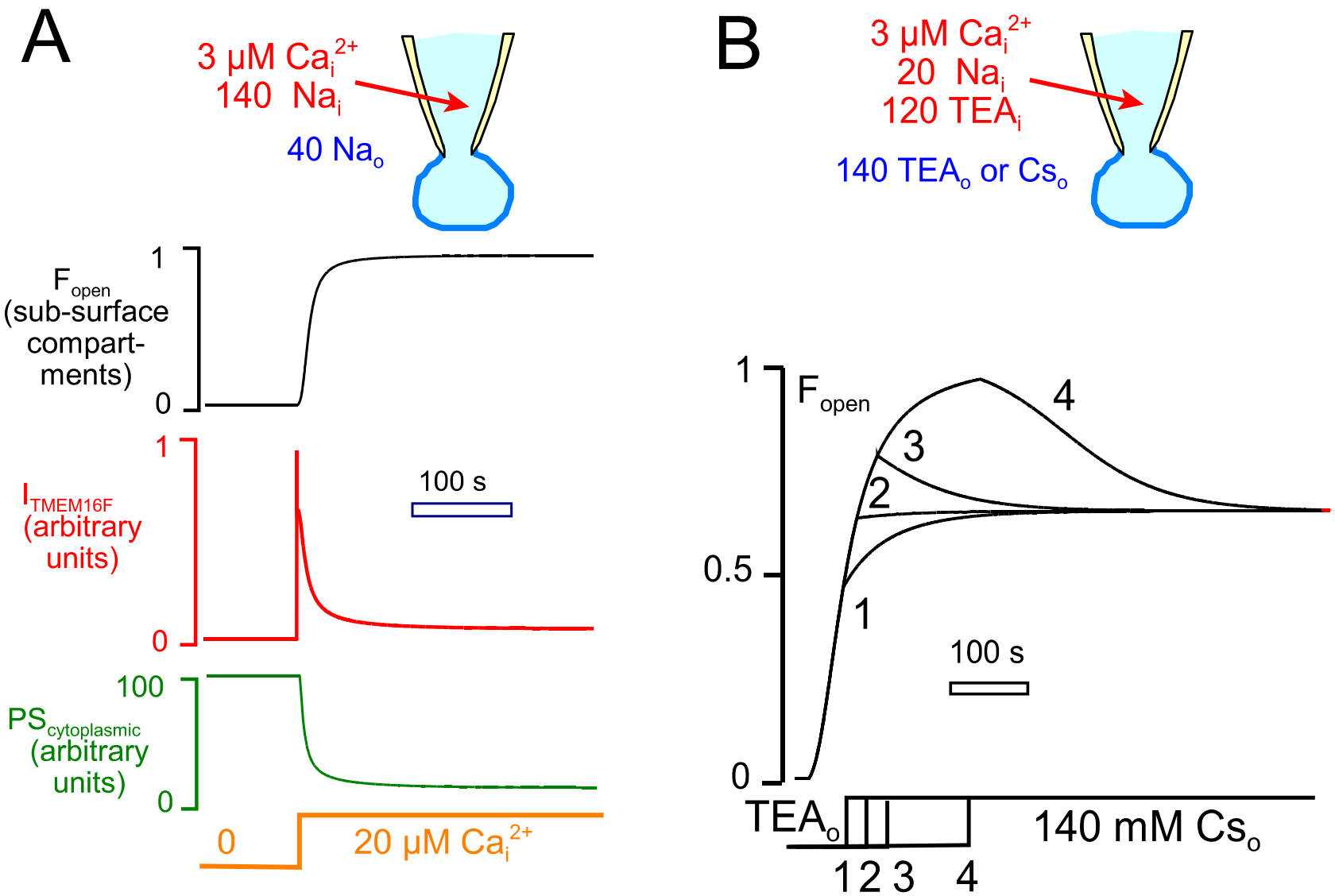
A
3 μM Ca$_i^{2+}$
140 Na$_i$
40 Na$_o$
F$_{open}$
(sub-surface compart-ments)
1
0
I$_{TMEM16F}$
(arbitrary units)
1
0
100 s
PS$_{cytoplasmic}$
(arbitrary units)
100
0
0
20 μM Ca$_i^{2+}$
B
3 μM Ca$_i^{2+}$
20 Na$_i$
120 TEA$_i$
140 TEA$_o$ or Cs$_o$
F$_{open}$
1
0.5
0
4
3
2
1
100 s
TEA$_o$
140 mM Cs$_o$
1 2 3 4

Fig. 8

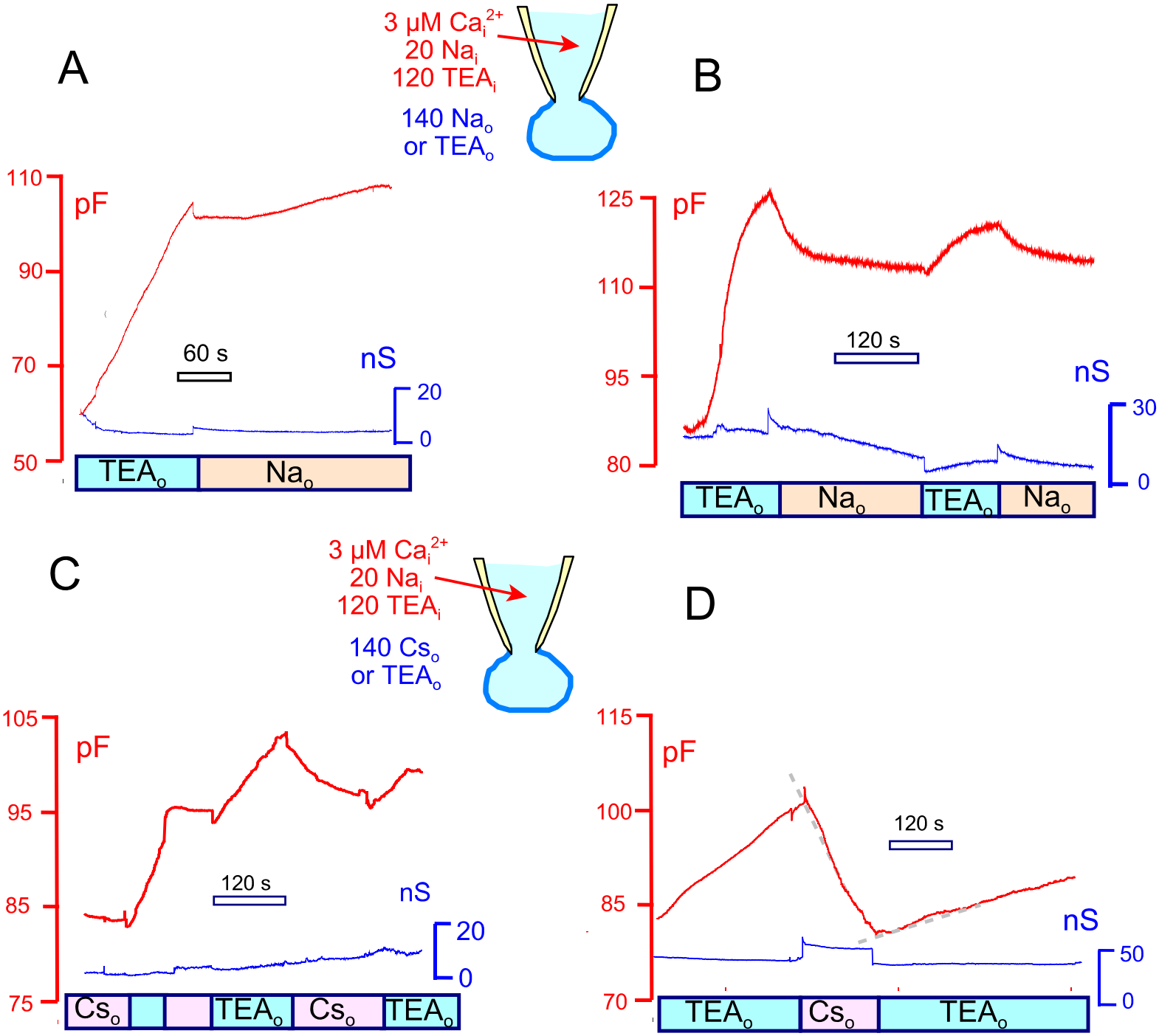
A
3 μM Ca$_i^{2+}$
20 Na$_i$
120 TEA$_i$
140 Na$_o$
or TEA$_o$
110
90
70
50
pF
60 s
nS
20
0
TEA$_o$
Na$_o$
B
125
110
95
80
pF
120 s
nS
30
0
TEA$_o$
Na$_o$
TEA$_o$
Na$_o$
C
3 μM Ca$_i^{2+}$
20 Na$_i$
120 TEA$_i$
140 Cs$_o$
or TEA$_o$
105
95
85
75
pF
120 s
nS
20
0
Cs$_o$
TEA$_o$
Cs$_o$
TEA$_o$
D
115
100
85
70
pF
120 s
nS
50
0
TEA$_o$
Cs$_o$
TEA$_o$

Fig. 9

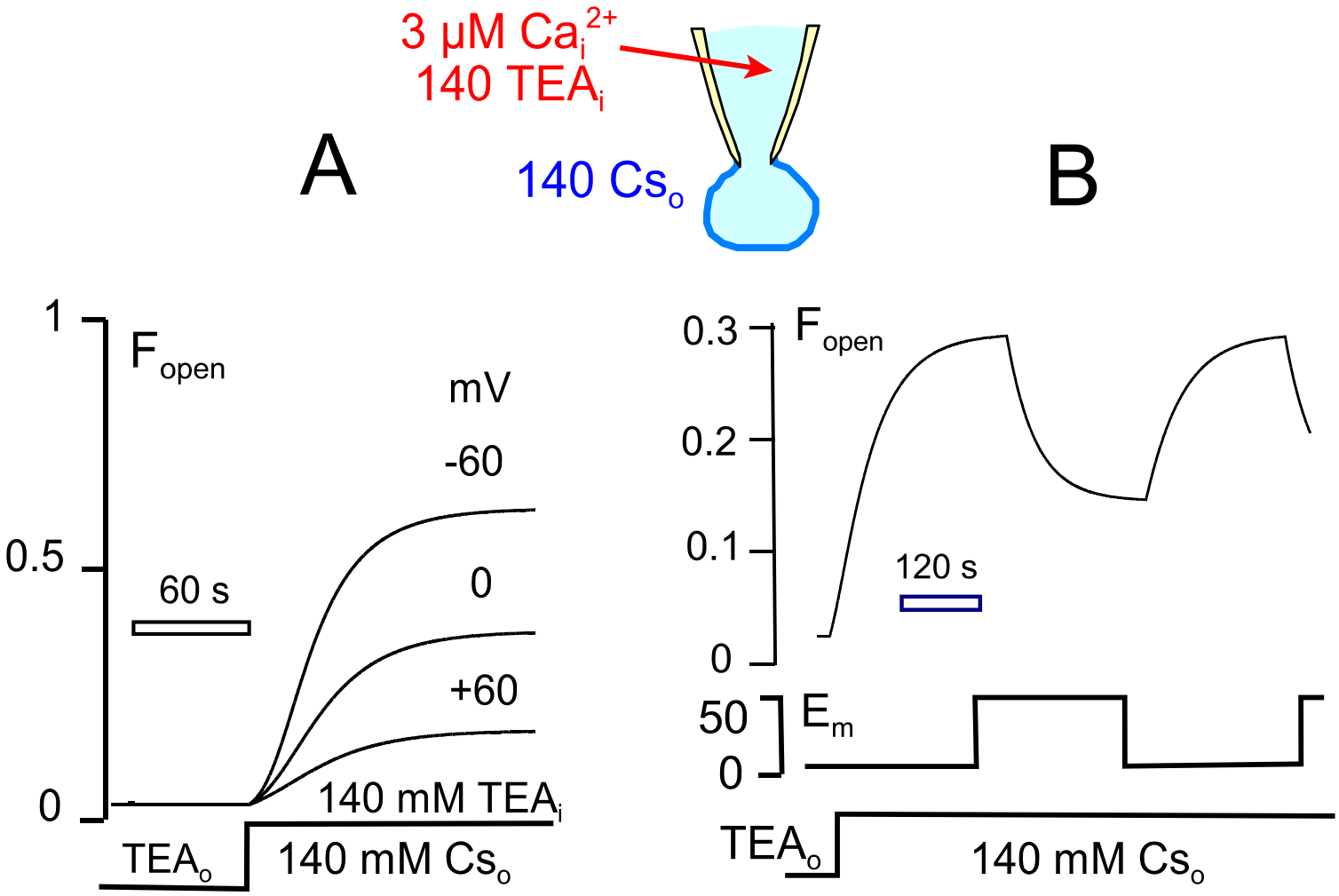
3 μM Ca$_i^{2+}$
140 TEA$_i$
140 Cs$_o$
A
B
1
0.5
0
F$_{open}$
mV
-60
0
+60
60 s
140 mM TEA$_i$
TEA$_o$
140 mM Cs$_o$
0.3
0.2
0.1
0
F$_{open}$
120 s
50
0
E$_m$
TEA$_o$
140 mM Cs$_o$

Fig. 10

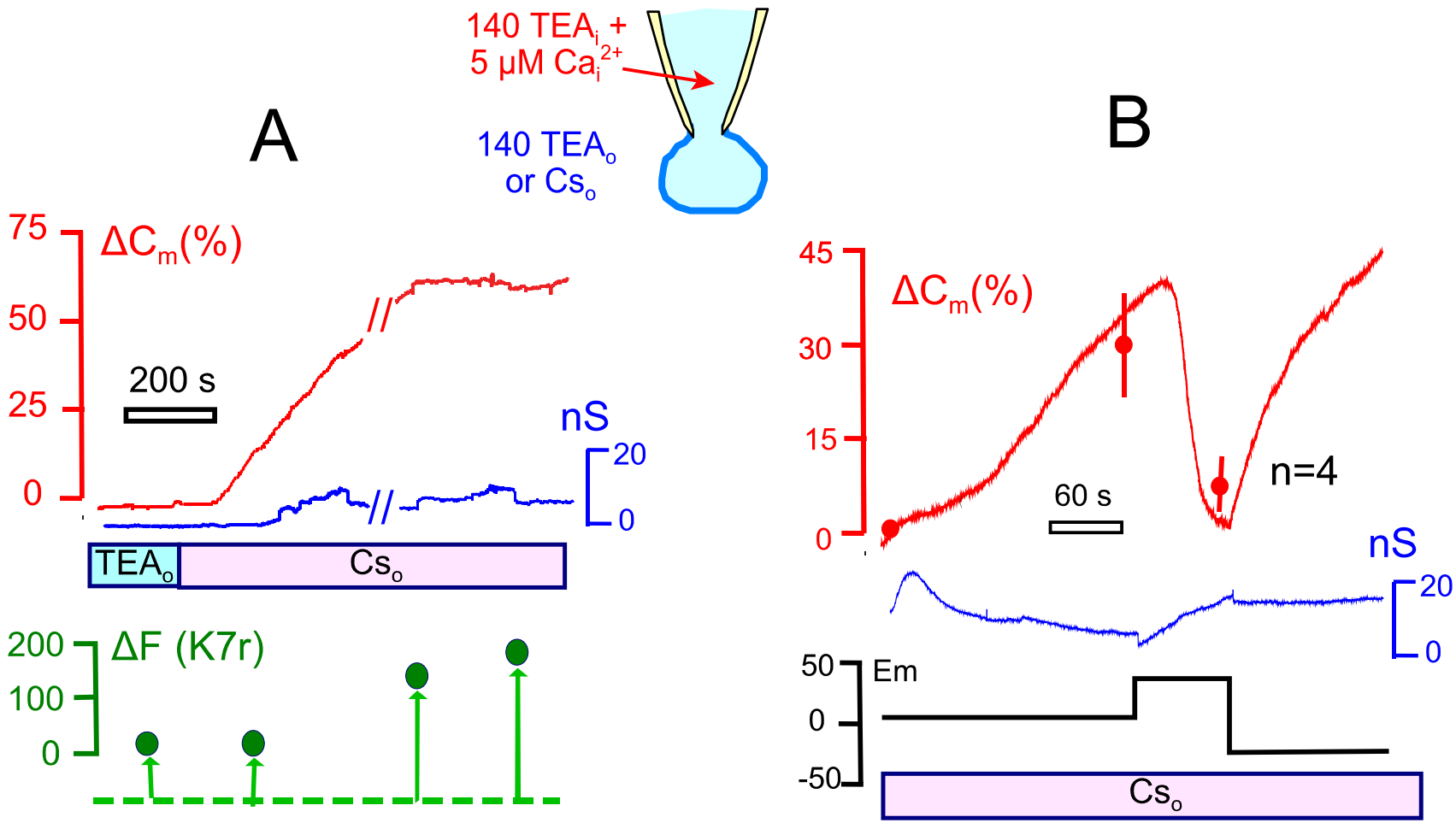
140 TEA$_i$ +
5 μM Ca$_i^{2+}$
140 TEA$_o$
or Cs$_o$
A
B
75
50
25
0
ΔC$_m$(%)
200 s
nS
20
0
TEA$_o$
Cs$_o$
200
100
0
ΔF (K7r)
45
30
15
0
ΔC$_m$(%)
60 s
n=4
nS
20
0
50
0
-50
Em
Cs$_o$

Fig. 11

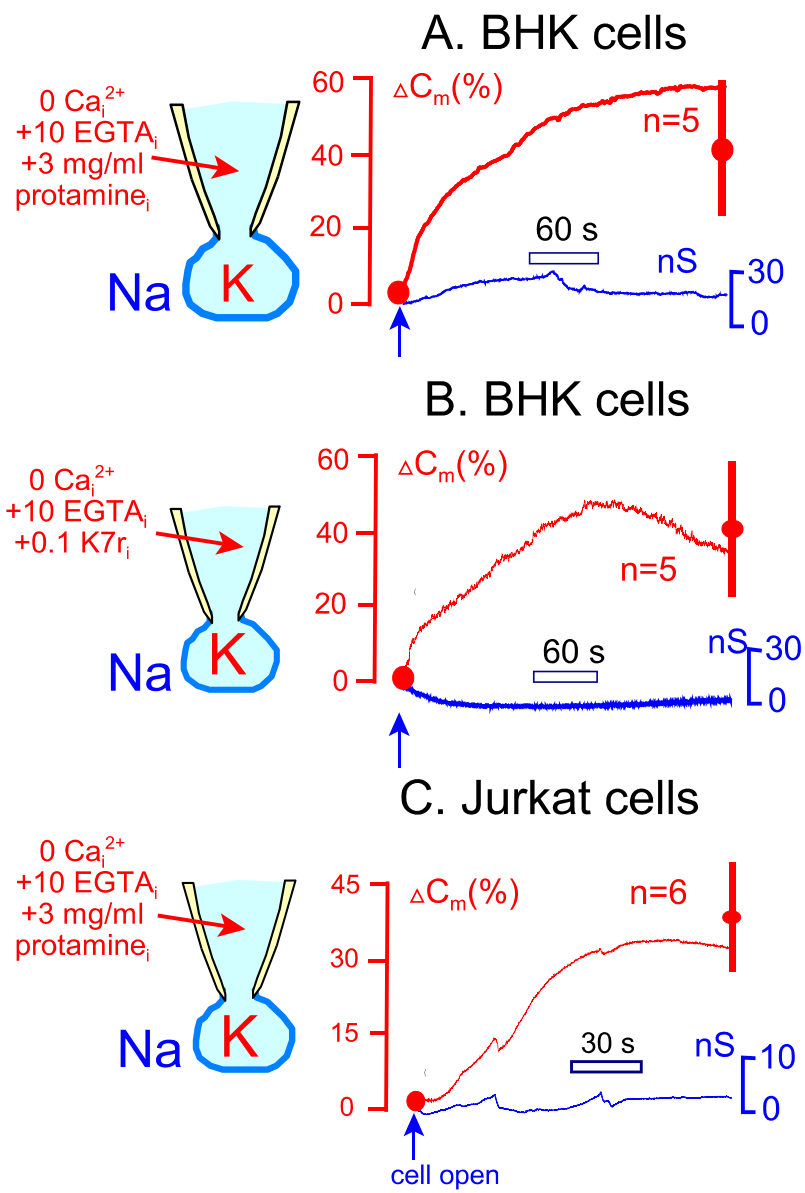
A. BHK cells
0 Ca$_i^{2+}$
+10 EGTA$_i$
+3 mg/ml
protamine$_i$
Na
K
60
40
20
0
ΔC$_m$(%)
n=5
60 s
nS
30
0
B. BHK cells
0 Ca$_i^{2+}$
+10 EGTA$_i$
+0.1 K7r$_i$
Na
K
60
40
20
0
ΔC$_m$(%)
n=5
60 s
nS
30
0
C. Jurkat cells
0 Ca$_i^{2+}$
+10 EGTA$_i$
+3 mg/ml
protamine$_i$
Na
K
45
30
15
0
ΔC$_m$(%)
n=6
30 s
nS
10
0
cell open

Fig. 12

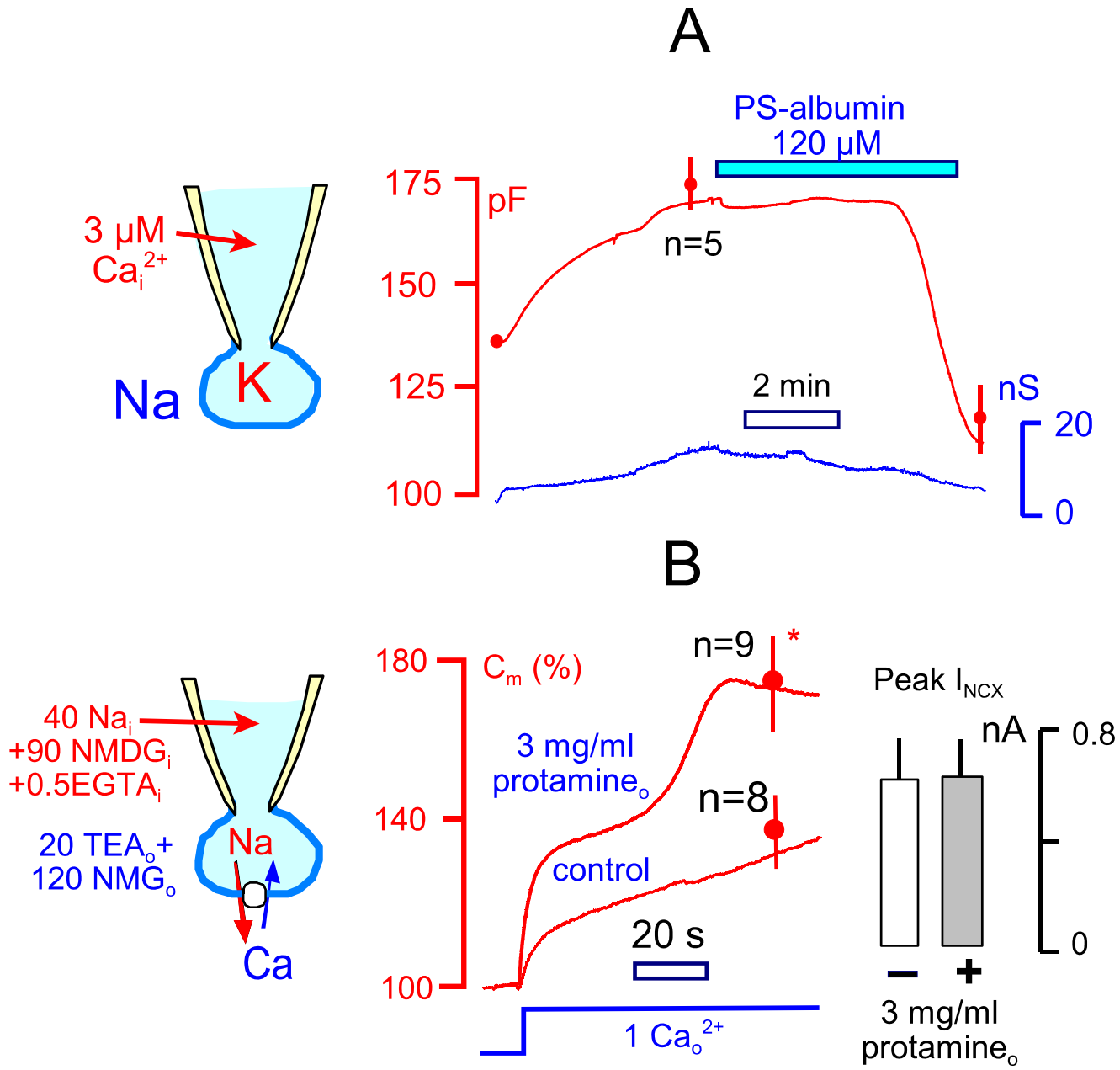
A
PS-albumin
120 μM
3 μM
Ca$_i^{2+}$
Na
K
175
150
125
100
pF
n=5
2 min
nS
20
0
B
40 Na$_i$
+90 NMDG$_i$
+0.5EGTA$_i$
20 TEA$_o$+
120 NMG$_o$
Na
Ca
180
140
100
C$_m$ (%)
n=9
*
3 mg/ml
protamine$_o$
n=8
control
20 s
1 Ca$_o^{2+}$
Peak I$_{NCX}$
nA
0.8
0
−
+
3 mg/ml
protamine$_o$

Fig. 13